

# UNCLASSIFIED

AD NUMBER
AD834469
NEW LIMITATION CHANGE
TO Approved for public release, distribution unlimited
FROM Distribution authorized to U.S. Gov't. agencies and their contractors; Critical Technology; 11 SEP 1967. Other requests shall be referred to U.S. Naval Ordnance Laboratory, White Oak, Silver Spring, MD.
AUTHORITY
NOL ltr, 15 Nov 1971

THIS PAGE IS UNCLASSIFIED

NOLTR 67-144

0834469

PRELIMINARY PARAMETRIC STUDY OF  
THE FLUTTER ARMING PRINCIPLE FOR  
FUZES

NOL

11 SEPTEMBER 1967

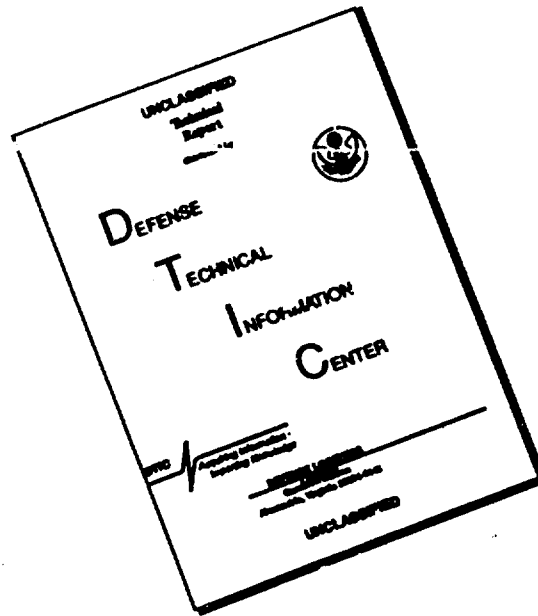
UNITED STATES NAVAL ORDNANCE LABORATORY, WHITE OAK, MARYLAND

NOLTR 67-144

This document is subject to special  
export controls and each transmittal  
to foreign governments may be made  
only with prior approval of NOL.

RECEIVED  
JUN 27 1968

# DISCLAIMER NOTICE



THIS DOCUMENT IS BEST QUALITY AVAILABLE. THE COPY FURNISHED TO DTIC CONTAINED A SIGNIFICANT NUMBER OF PAGES WHICH DO NOT REPRODUCE LEGIBLY.

NOLTR 67-144

PRELIMINARY PARAMETRIC STUDY  
OF THE FLUTTER ARMING PRINCIPLE  
FOR FUZES

Prepared by:  
P. D. Gratton

**ABSTRACT:** The Flutter Arming Mechanism (FAM) principle is a controlled flutter phenomenon. A rectangular flat plate oscillating member is pivoted about its midchord on a member providing a flexural restoring moment. Placed edgewise in an air stream, the system is in unstable-stable equilibrium; at a predetermined air speed or above, aerodynamic lift on the front portion of the flat plate overcomes the flexural resisting moment and the oscillator vibrates. The vibrations occur at the natural frequency of the oscillator-flexural member combination. Wind tunnel data are presented which indicate the FAM principle has the necessary basic criterion of a time base, velocity discriminating mechanism required for bomb and bomblet fuze application.

Published  
11 SEPTEMBER 1967

U. S. NAVAL ORDNANCE LABORATORY  
WHITE OAK, MARYLAND

NOLTR 67-144

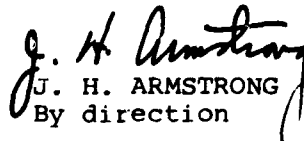
11 September 1967

PRELIMINARY PARAMETRIC STUDY OF THE FLUTTER ARMING PRINCIPLE FOR FUZES

This report is the first in a series of reports to be generated covering the parameters and functioning of the flutter arming principle. It represents the first parametric study conducted with the scope limited to first approximations and verifications of such in actual wind tunnel tests. It is useful to the extent that a solid basis has now been established for designing a more refined series of tests and test devices to aid in the development of this new concept for fuze application. This work was performed under AIRTASK No. A35-532-006/292-1/F008-08-07.

It is a pleasure to acknowledge the cooperation of Virginia Schermerhorn of the Naval Ordnance Laboratory, Applied Aerodynamics Division, for her interpretation and comments of the wind tunnel data.

E. F. SCHREITER  
Captain, USN  
Commander

  
J. H. ARMSTRONG  
By direction

CONTENTS

	Page
INTRODUCTION.....	1
SYMBOLS.....	1
THEORY.....	2
TEST SETUP.....	3
PARAMETERS.....	3
INSTRUMENTATION.....	4
CALCULATIONS.....	4
RESULTS.....	9
COMMENTS.....	12
CONCLUSIONS.....	13
APPENDIX A.....	A-1
APPENDIX B.....	B-1

ILLUSTRATIONS

Figure	Title	
1	Control Volume Model.....	15
2	Oscillator Configuration.....	16
3	Space Locations In Control Volume Model.....	17
4	Typical Frequency of Vibration with Oscillator Downstream Location as Parameter.....	18
5	Frequency Response as a Function of Oscillator Location with $\bar{A}_c/A_t = 9.5$ .....	19
6	Frequency Response with Chamber Velocity as Parameter Showing Optimum "d" Location.....	20
7	Blunt Leading Edge Oscillator at Near Optimum "d" Location.....	21
8	Frequency Response as a Function of Oscillator Location with $\bar{A}_c/A_t = 7.4$ .....	22
9	Frequency Response at an Oscillator "d" Location of .188 in.....	23
10	Frequency Response for d = .280 with $\bar{A}_c/A_t$ as Parameter	24
11	Frequency Comparison Between Blunt and Round Leading Edged Oscillator.....	25
12	Frequency Response For a Balanced One-Half Oscillator From Mach .15 to Mach 1.12.....	26
13	Chamber Velocity as a Function of Inlet Velocity For Various $A_i/A_t$ Ratios.....	27
14	Typical Chamber Air Densities as a Function of Chamber Velocities.....	28
15	Typical Chamber Velocity Relationship to Angle of Attack	29
16	Energy Gradient Concept.....	30
17	Optimum Control Volume Configuration For Constant Frequency Oscillator Response.....	31

ILLUSTRATIONS (contd)

Figure	Title	Page
3-1, B-5	Frequency Response with Oscillator Downstream Location as Parameter.....	B-1, B-5
3-6	Frequency Response For $\frac{A_c}{A_t} = 5.2$ ; $d = .280$ .....	B-6
3-7	Frequency Response for $\frac{A_c}{A_t} = 7.4$ ; $d = .280$ .....	B-7
3-8	Frequency Response For a Round Leading Edge Oscillator.....	B-8

REFERENCES

- (a) Paper #45 entitled: "Flutter Arming and Timing Mechanism For Fuzes" by P. D. Gratton and W. J. Donahue presented at the Timers For Ordnance Symposium, Washington, D. C. on 15-16 Nov 1966 sponsored by Harry Diamond Laboratory. This reference is available through the Defense Documentation Center
- (b) Handbook of Chemistry and Physics, 40th Ed p. 2121
- (c) National Advisory Committee For Aerodynamics Report #1135, p. 21, Table 1
- (d) Strength of Materials by Ferdinand L. Singer p. 213
- (e) "Applied Aerodynamics," by Leonard Bairstow p. 416

## INTRODUCTION

1. The components in a conventional mechanical fuzing system for bombs include an arming vane\* to extract energy from the environment, high speed bearings to insure proper rotational characteristics of the arming vanes, clutch or similar mechanism to sense a specific velocity threshold and a clock escapement or governor for proper delay arming of the fuze. This technical report is concerned with another mechanism that current exploratory development shows to have promise for accomplishing the same ends. At a minimum velocity and above, controlled vibrations from a flat plate pivoted about its midchord provide a constant frequency time base mechanism. The arming vanes, high speed bearings and clock escapement or governor are eliminated. The mechanism has the potential of becoming an inexpensive environmentally operated delay arming device that could effect a considerable saving when used on fin stabilized ordnance.

2. This fuze arming mechanism, which is based on the phenomenon of aerodynamic flutter, is known as the Flutter Arming Mechanism (FAM). Studies of the FAM were conducted in the wind tunnel by the use of a special model of the FAM referred to as the control volume model. This model was so constructed that certain fundamental parameters could be changed from test to test to study the effects of the change. This model was not intended to represent any scale fuze design but idealizes the operational environment and air flow considerations. The information obtained from this model will be applied to fuze design models in the future. The majority of the data presented were for subsonic tunnel speeds but some supersonic runs were conducted.

## SYMBOLS

3. For convenience in reference all symbols used in subsequent paragraphs are defined here.

$\bar{a}$  = distance from pivot point to center of pressure (in.)  
 $a^*$  = speed of sound at throat (ft/sec)  
 $f$  = natural frequency (Hz)  
 $q_c$  = chamber dynamic pressure (psi)  
 $\bar{A}_c$  = average chamber area (in.)  
 $A_c$  = chamber area (in.)  
 $A_i$  = inlet area (in.)  
 $A_t$  = throat area (in.)  
 $C_N$  = aerodynamic lift coefficient  
 $E_w$  = Young's Modulus,  $30 \times 10^6$  psi  
 $I_w$  = oscillator moment of inertia (lb-in.-sec<sup>2</sup>)  
 $I_w$  = inertia of wire (in.<sup>4</sup>)  
 $K$  = spring constant (lb-in./rad.)

\* typically a rotating propeller or turbine, axial or radial flow



$M$  = Mach number  
 $M_a$  = Aerodynamic Moment  
 $P_c$  = chamber static pressure at leading edge of oscillator  
 $S$  = surface area of oscillator (in.<sup>2</sup>)  
 $V_c$  = chamber velocity at leading edge of oscillator (ft/sec)  
 $V_i$  = inlet or upstream air velocity (ft/sec)  
 $V_{cr}$  = chamber velocity at threshold (ft/sec)  
 $Z$  = length of wire between supports (in.)  
 $\alpha$  = angle of attack  
 $\rho_c$  = chamber air density at leading edge of oscillator (lb-sec<sup>2</sup>)/ft<sup>4</sup>  
 $\rho_i$  = inlet air density (lb-sec<sup>2</sup>)/ft<sup>4</sup>  
 $P_i$  = inlet static pressure (cm of mercury)  
 $P_{ti}$  = inlet total pressure (cm of mercury)  
 $P_{tc}$  = chamber total pressure (cm of mercury)  
 $t$  = temperature °C  
 $d$  = location of oscillator leading edge from nozzle exit (in.)

#### THEORY

4. The unstable divergent motion witnessed by wing and tail sections on some aircraft is a type of vibration that once started at a critical speed the end result is an ultimate structural failure. Another extreme would be the damped motion where at first member would vibrate when excited but internal and external damping causes gradual subsiding of motion in a finite amount of time. The FAM principle is an unstable oscillating type or controlled flutter mechanism between these two extremes (continuous motion with no change in amplitude).

5. The control volume model has a flat plate or oscillator pivoted and balanced about its midchord located in a parallel walled chamber. A restoring spring is attached at the pivot axis to give bias zero point of reference. An air stream impinging the leading edge of the oscillator will create an aerodynamic lifting force that works at the center of pressure (c.p.) tending to rotate the oscillator from the zero reference point. Only at a threshold speed and above will the aerodynamic lifting forces be sufficient to overcome the spring restoring moment causing the oscillator to rotate to a stall position (approximately 10 degrees). At stall the aerodynamic lift is essentially zero but the restoring spring has acquired internal energy (due to bending) that causes the oscillator to return to a reference point. However, the oscillator inertia causes a slight overshoot past the reference point allowing the aerodynamic forces to build up on the reverse face. The oscillator rotates to a -10 degree position (stall) and a controlled cyclic pattern of amplitude and frequency is established. The frequency of vibration should be the natural undamped frequency of the oscillator-restoring member combination. A balance between the oscillator inertia, elastic properties of the restoring member, and the aerodynamic forces can

give various threshold velocities for starting vibration along with constant frequencies for a time base. The described system is a simplified explanation of the FAM operation. In actual application the control volume model has a convergent nozzle that directs the air flow to the leading edge of the oscillator. The aerodynamic forces applied to the oscillator are changed by the addition of the nozzle. The lift is destroyed at "stall" due in part to the oscillator hiding behind part of the nozzle or out of the effective air flow.

#### SETUP

6. Figure 1 shows the relative size and location of the various components of the control volume model. The housing was mounted on a 15" sting and this in turn was mounted on a rotating sector arm in the wind tunnel. The purpose of this setup was to rotate the control volume model through angles of attack yet keep the leading edge of the oscillator in the center of the wind tunnel section.

7. The plane of the oscillator in the control volume model is normally horizontal; this is referenced to a zero angle of attack. A 20 degree angle of attack is characterized when the control volume model is rotated 20 degrees from the horizontal. Figure 2 shows the size and configuration of the blunt oscillator used for the majority of the tests.

8. The restoring member (.016 diameter music wire) was used in all the tests. Wire breakage was common after an average of four to five tunnel runs (about 7.5 seconds per run), especially at the high subsonic Mach numbers.

9. The channeling or nozzling is needed to obtain a constant frequency of vibration over the velocity and angle of attack range. The need has been demonstrated in previous tests (ref. (a)). Various nozzle openings were inserted and adjusted to change the inlet-to-throat and chamber-to-throat ratios.

#### PARAMETERS

10. The major parameters that influence the functioning of the oscillator are the area opening ratios and the distance from the nozzle exit aft to the leading edge of the oscillator. The area opening ratios refer to the inlet-to-throat areas ( $A_i/A_t$ ) and the average chamber-to-throat areas ( $A_c/A_t$ ). These variables were readily changeable with slide-in-type nozzles (oscillator remaining in the same position). For space locations see Figure 3.

11. The inlet air speed was varied from 75 to 690 knots to determine frequency response and threshold velocities.

12. The angle of attack on the oscillator in the control volume model was swept through angles of attack starting from -6 and ending at 20 degrees. This range was the physical limit of the sector arm in the tunnel and represents an adequate fuze functioning range.

13. The majority of tests had a blunt leading edged oscillator but a few runs were made with a rounded leading edge, the radius being one-half the oscillator thickness. (See Figure 2.)

# INSTRUMENTATION

14. For frequency measurements a magnetic transducer was inserted in the housing just over the aft end of the oscillator. As the oscillator moved through the flux lines set up by the magnet, a flux change and in turn voltage change were permanently recorded by two systems. For immediate read out, an X-Y plotter was used. For more sophisticated and accurate information the data was put on tape (Digital Analog Recording Equipment) to be analyzed at a later date. The frequency was recorded as a function of time and angle of attack.

15. Oscillator rise time was measured using the transducer and visocorder. A carrier frequency (100 Hz) was recorded simultaneously with the transducer output on light sensitive paper. Comparing the two outputs gave the corresponding rise time.

16. Amplitude of oscillation was recorded on film using a dial indicator attached to the oscillator shaft. The film could be later analyzed for exact displacements. An "E" core-type system will be used in the future to record both amplitude and frequency simultaneously. Visual amplitude was constant at  $\pm 10^\circ$ .

17. Wind tunnel supply pressures  $P_{t1}$ , tunnel static pressures  $P_s$  and temperatures  $t$  were also measured and recorded with Digital Analog Equipment. The control volume model chamber static pressure was measured with a pressure tap located half in the air directly in front of the oscillator and the other half of the tap over the oscillator.

# CALCULATIONS

18. The calculated frequency of oscillator vibration is the natural frequency of the oscillator inertia and the restoring member combination. This frequency is for a no-load output; no gears, ratchet or power take-off from the oscillator to perform the fuze arming and arming function will be considered at this time. The frequency would adjust to a lower value if the gear inertia, ratchet efficiency and bearing friction are considered in the oscillator inertia term.

$$f = \sqrt{\frac{K}{I}}$$

Equation (1)

where  $K = 12 \frac{E_w I_w^3}{Z}$

for ".016 dia.  $I_w = .322 \times 10^{-8} \text{ in}^4$

$E_w = 30 \times 10^6 \text{ psi}$

$Z = 1.140 \text{ in}$

$K = 102.0 \times 10^{-2} \text{ lb-in}$

and  $I = .2215 \times 10^{-4} \text{ lb-in-sec}^2$

$$f = \left[ \frac{102.0 \times 10^{-7}}{.2215 \times 10^{-4} \text{ sec}^2} \right]^{\frac{1}{2}}$$

$$= 216.0 \frac{\text{rad}}{\text{sec}}$$

$$\text{or } f = \frac{1}{2\pi} (216.0) \text{ Hz} \\ = 34.4 \text{ Hz}$$

<sup>1</sup> Derivation of this relationship is presented in Appendix A.

19. The chamber velocity, ( $V_c$ ), at the leading edge of the oscillator can be calculated knowing the physical dimensions of the nozzle and the inlet air velocity and density.

$$q_c = \frac{1}{2} \rho_c V_c^2 \quad \text{dynamic pressure} \quad \text{Equation (2)}$$

$$\text{Reversible} \quad q_c/p_c = \frac{\gamma}{\gamma+1} \left( \frac{V_c}{a^*} \right)^2 \left[ 1 - \left( \frac{\gamma-1}{\gamma+1} \right) \left( \frac{V_c}{a^*} \right)^2 \right]^{-1} \quad \text{Equation (3)}$$

where  $P_c$  = chamber static pressure  
(measured with pressure tap)

$a^*$  = speed of sound at throat

$$(49 \sqrt{.833 t_o})$$

for air  $\gamma = 1.4$   
Eq. 3 becomes

$$q_c/p_c = \frac{7}{12} \left( \frac{V_c}{a^*} \right)^2 \left[ 1 - \frac{1}{6} \left( \frac{V_c}{a^*} \right)^2 \right]^{-1} \quad \text{Equation (3A)}$$

Continuity

$$\rho_c V_c = \rho_1 V_1 A_1 / A_c \quad \text{Equation (4)}$$

where 1 designates free stream  
or inlet conditions;  $A_c$  = average  
cross section where pressure tap  
is located.

Substituting Equation 2 into Equation 3A and Equation 4 into 3A  
we have:

$$\frac{1}{2} \left( \rho_1 V_1 A_1 / \bar{A}_c \right) \frac{V_c}{P_c} = \frac{7}{12} \left( \frac{V_c}{a^*} \right)^2 \left[ 1 - \frac{1}{6} \left( \frac{V_c}{a^*} \right)^2 \right]^{-1}$$

or

$$\left[ \frac{6}{7} \left( \rho_1 V_1 A_1 / \bar{A}_c \right) \frac{a^*}{P_c} \right] \left[ 1 - \frac{1}{6} \left( \frac{V_c}{a^*} \right)^2 \right] - V_c = 0 \quad \text{Equation (5)}$$

which is in quadratic form and easily solvable. Attention is fixed to the positive answer only

$$V_c = \frac{-b + \sqrt{b^2 - 4ac}}{2a}$$

20. The  $\bar{A}_c$  term used in Equation 5 and noted on the Figures differs slightly from the term  $A_c$ . The difference is slight but for accurate  $V_c$  calculations it must exist. The chamber static pressure probe located over the oscillator and partly in the free stream reads an average pressure over these two extremes. The  $\bar{A}_c$  term is therefore an average chamber area corresponding to the average static pressure reading.

21. The chamber stagnation pressure  $P_{tc}$  can be calculated using the isentropic equation behind the shock wave,

$$P_{tc} = P_c \left[ 1 - \frac{1}{6} \left( \frac{V_c}{a^*} \right)^2 \right]^{-7/2} \quad \text{Equation (6)}$$

22. The inlet and chamber dynamic air densities were calculated from a thermally perfect dry air equation, (ref.(b))

$$\rho_t = \frac{0.001293 H}{1 + 0.00367 t} \frac{\text{grams}}{\text{milliliter}} \quad \text{Equation (7)}$$

where H = inlet ( $P_t$ ) or chamber ( $P_{tc}$ ) total pressure (cm)

t = temperature °C

23. Calculating the  $P_c/P_{tc}$  ratio and referring to ref.(c) a Mach number in the chamber and a ratio of static density/dynamic density ( $\rho_c/P_{tc}$ ) can be obtained. The static chamber density can then be found by multiplying the  $\rho_c/P_{tc}$  ratio by  $P_{tc}$  (Equation 7). The static chamber density was used in calculating the threshold or starting velocity.

24. The threshold or start-up velocity can be calculated knowing the restoring spring physical properties and the aerodynamic moment causing deflection.

Critical or Start-up velocity:

Restoring Spring Moment = Aerodynamic Moment

$$K\alpha = \left( C_N \frac{1}{2} \rho_c V_{cr}^2 \right) S\bar{a} \quad \text{Equation (8)}$$

$C_N = 2\pi\alpha$  for a flat plate

$$K\alpha = 2\pi\alpha \left( \frac{1}{2} \rho_c V_{cr}^2 \right) S\bar{a}$$

$$V_{cr}^2 = \frac{K}{\pi \rho_c S\bar{a}}$$

$$K = 102.0 \times 10^{-2} \text{ lb-in.}$$

$$S = 1.19 \text{ in}^2$$

$$V_{cr} = \left[ \frac{1.02 (144)}{1.19 \pi} \right]^{\frac{1}{2}} \sqrt{\frac{1}{\rho_c \bar{a}}}$$

$$\text{where } \rho_c = \frac{\text{lb} - \text{sec}^2}{\text{ft}^4}$$

$$\bar{a} = \text{in.}$$

$$V_{cr} = [39.3]^{\frac{1}{2}} \sqrt{\frac{1}{\rho_c \bar{a}}}$$

$$V_{cr} = 6.25 \sqrt{\frac{1}{\rho_c \bar{a}}}$$

$$\text{let } \rho_c = 2.16 \times 10^{-3} \frac{\text{lb} - \text{sec}^2}{\text{ft}^4}$$

$$\bar{a} = .465 \text{ in}$$

$$V_{cr} = 6.25 \sqrt{\frac{1}{2.16 \times 10^{-3} .465}}$$

$$V_{cr} = 205. \text{ ft/sec or 121 Knots chamber velocity}$$

25. Certain parameters regarding the aerodynamic lift should be mentioned.

a. The lift coefficient,  $C_N$ , for a flat plate is in general  $2\pi\alpha$  for ideal flow conditions. The flow is not ideal in this application due to the diffuser effect as the air enters the oscillator chamber. The disturbed air flow along with the oscillator thickness and leading edge configuration will have some influence on the lift coefficient.

b. Another general assumption that has been made deals with the center of pressure,  $\bar{a}$ , location. A quarter chord from the leading edge is the assumed location, regardless of the angle of attack. Like all wing sections the c.p. for the flat plate will shift when the angle of attack changes.

c. The magnitude of the aerodynamic lift and moment on the oscillator can be altered by the presence and location of the confining chamber walls. Present information (ref.(e)) indicates a maximum of 32% increase in lift can be realized for an oscillator chord to chamber wall separation ratio of 1. The trend is toward an increasing lift coefficient for greater chord/wall ratios. The information did not include the physical limits of the control volume model configuration of chord/wall=2.8 so this correction will not be made. The calculated threshold chamber velocity is 121 knots.

d. The compressibility factor of air was not taken into account for Equation 8. The error amounts to approximately 2% of the threshold at 121 knots chamber velocity but will be significantly greater percentage of error at the high subsonic speeds.

26. At a fixed tunnel air speed or inlet air speed, the air is accelerated as it approaches the throat of the convergent nozzle. The air flow is accelerated to a limiting value of the speed of sound or Mach 1 at the throat. Using inlet and throat dimensions for the nozzle, the inlet air velocity ( $V_1$ ) establishing Mach 1 at the throat can be calculated as shown by Equation (9).

For Mach 1 at the throat:

$$V = \frac{a^*}{A_1/A_t} \quad \text{Equation (9)}$$

$$a^* = 1010 \text{ ft/sec} \quad A_1/A_t = 5.6$$

$$V_1 = \frac{1010}{5.6} = 180.5 \text{ ft/sec}$$

$$V_1 = 107 \text{ knots}$$

## RESULTS

27. Figure 4 shows the frequency response at angles of attack for a blunt leading edge oscillator for a particular chamber and inlet ratio. The figure is typical of the results for each nozzle configuration and oscillator location and the remaining figures similar to Figure 4 are shown in Appendix B. It is important to note on the curves that the frequency response is relatively constant at angles of attack from  $-6$  to  $20$  degrees for each run.

28. Figure 5 is a summary of Figures 4 and Figures B-1 through B-5 of Appendix B, showing the oscillator downstream location "d" from the nozzle as parameter with frequency and inlet velocity as variables. The curves are for  $A_1/A_t = 5.6$ ,  $\bar{A}_c/A_t = 9.4$  and the frequency values are taken at near zero degree angle of attack. The following observations can be made from this summary:

a. As the inlet velocity increases a linear divergence of frequency for the family of curves exists. Within limits, the closer the oscillator is to the nozzle exit the greater the frequency is at the higher inlet speeds. The further away the oscillator is located the lower the frequency becomes at higher inlet air speeds. The various downstream oscillator locations indicate an optimum location for constant frequency.

b. The family of curves can be extended until a point of intersection is reached. Providing the linearity exists in this region, the point of intersection should indicate the threshold or starting velocity at the systems natural frequency. The intersection point is at the calculated frequency and also indicates a threshold of 103 knots inlet velocity. More detail is observed from Figure B-1 of Appendix B showing a 70 knot no-go, 95 knot imminent and 118 knot go situation.

29. Figure 6 shows the same summary as Figure 5 but the parameter is the inlet velocity plotted against the frequency and downstream oscillation location. The point in common for the four curves indicates an optimum "d" location for a constant frequency. For the particular nozzle configuration and  $A_1/A_t$   $\bar{A}_c/A_t$  ratios, the oscillator location is .232 in. downstream of the nozzle exit. The intersection point of the curves coincides with the calculated natural frequency (error of .4  $H_z$ ).

30. Figure 7 shows the frequency response against inlet air speed at an oscillator location of .222 in. downstream of the nozzle. The frequency starts at the calculated natural frequency (34.4  $H_z$ ) and is driven to 36.0  $H_z$  at 500 knots inlet velocity. The oscillator location was slightly closer to the nozzle than the optimum dimension (Figure 6) so a slight driving of the frequency at high inlet speeds is expected. The  $A_1/A_t$  and  $\bar{A}_c/A_t$  ratios for Figure 7 differs slightly from Figure 5.



31. Figure 7 also shows the starting velocity as 105 knots inlet air speed. Air speeds below 105 knots did not start the oscillator even when rotated through angles of attack from -6 to 20 degrees. Mach 1 at the throat for this  $A_1/A_t$  ratio was calculated at 117 knots.

32. Figure 8 shows the frequency response with oscillator downstream location as parameter for constant  $A_1/A_t = 5.1$  and  $\bar{A}_C/A_t = 7.40$ . The frequency starts at the natural frequency and then diverges similar to Figure 5.

33. Comparing the results of Figure 5 to Figure 8 shows little difference for the frequency response for assumed constant  $A_1/A_t$  but different  $\bar{A}_C/A_t$  ratios at reasonable oscillator locations. Placement of the oscillator too far from the nozzle will eventually lead to a non-vibrating condition at high subsonic air speeds. If the oscillator is placed too close to the nozzle a condition indicated by Figure 9 is generated. The frequency response is erratic varying from 0 to 55 Hz.

34. Figure 10 (summary of Figures B-3, B-6 and B-7 of Appendix B) shows the frequency trends for different  $\bar{A}_C/A_t$  ratios. The oscillator location was .280 in., near the optimum "d" dimension of .232. For comparison reasons only the  $A_1/A_t$  ratios will be considered constant even though they varied from 5.5 to 4.53. The figure indicates a reasonable frequency response at  $\bar{A}_C/A_t$  ratios of 9.5 to 7.4; however, at an  $\bar{A}_C/A_t$  of 5.2 the frequency has a significant drop-off.

35. Tests were conducted comparing the response of a rounded leading edge oscillator to a blunt leading edge. Figure 11 shows the results for an oscillator location of .222" and ratios of  $A_1/A_t = 5.07$  and  $\bar{A}_C/A_t = 7.4$ . Of the two configurations the rounded oscillator had a 30 knot lower starting velocity than did the blunt leading edge oscillator. The frequency of vibrations at threshold velocity was the systems natural frequency (34.4 Hz) for both leading edge configurations. Both had divergence as the inlet air speed increased but more so for the rounded configuration. The blunt leading edge went to 35.7 Hz and the round leading edge to 39 Hz at 500 knots inlet. (Figure 11 is a comparison of Figures 7 and B-8).

36. A configuration was tested that had the aft end of a blunt leading edge oscillator removed. A counterweight located out of the air stream was added to dynamically balance the remaining half. The intent of the setup was to demonstrate whether or not the FAM concept would work with just the front half of the oscillator thus conserving space for fuzing applications. The blunt leading edge oscillator was .063 thick as compared to the .088 thick oscillator in the other tests. A .203 in. oscillator "d" location was used with  $A_1/A_t = 4.58$  and  $\bar{A}_C/A_t = 7.75$ . The results of the test are shown on Figure 12. The threshold for this configuration is estimated at 250 knots with oscillator vibration continuing to 690 knots (Mach 1.15) inlet velocity. Unfortunately no real assessment of the higher

starting velocity for the one-half balanced oscillator can be made. Had a #063 thick full oscillator been tested, a direct comparison would be possible. The effect of the oscillator cross-sectional area on frequency response is not known. The theoretical starting velocity was calculated at 135 knots chamber or 195 knots inlet. (Appendix A.) The starting vibrations were 38  $H_z$ , slightly lower than the systems calculated natural frequency of 40.4  $H_z$ . As the inlet velocity increased, the vibrations increased to 42  $H_z$  for an inlet velocity equal to Mach 1. The chamber velocity at the leading edge was calculated at 400 knots for a free stream Mach 1. After this point, the frequency dropped to 39  $H_z$  at 690 knots inlet or 475 knots chamber velocity.

37. The rise time for the #088 thick blunt oscillator to attain its natural frequency was measured at .005 sec. at threshold velocity. The oscillator "d" location was .280 in. with  $A_i/A_t = 5.6$  and  $\bar{A}_c/A_t = 9.5$ . The rise time is for a no-load work output condition and measured from a relative zero degree starting point to a 10 degree maximum oscillator movement (1/4 cycle). The calculated rise time for the oscillator to go 1/4 cycle at a natural frequency of 34.4  $H_z$  is .0073 sec. The difference between the actual and calculated rise times can be attributed to 1) the oscillator did not start at a 0 degree angle of attack, so something less than a 1/4 cycle was actually witnessed and 2) the rise time was measured at tunnel start-up where pressure surges of 2 or 3 times steady state conditions exist. It should be noted that the slowest rise time expected (no-load) should be based on the natural frequency 1/4 cycle calculation.

38. Figure 13 shows the chamber velocity as a function of the inlet velocity with  $A_i/A_t$  as the parameter. The calculated threshold velocity is 121 knots chamber or 200 knots inlet for  $A_i/A_t = 5.6$ . The actual threshold determined through tests was 103 knots inlet (Figure 5) for a blunt oscillator at  $d = .280$  in. The actual starting velocity almost coincides with Mach 1 at the throat. For the blunt oscillator with  $d = .222$  and a  $A_i/A_t = 5.1$  (Figure 8) the same calculated chamber velocity indicates the inlet threshold should be 160 knots. The actual inlet velocity was found to be 105 knots (Figure 7). Once again the actual threshold approaches the velocity where Mach 1 is established at the throat.

39. Figure 14 shows the typical change of the static chamber air density as a function of the chamber velocity. The density change over the velocity range is significant ranging from .0022 lb-sec<sup>2</sup>/ft<sup>4</sup> at 100 knots to .0014 lb-sec<sup>2</sup>/ft<sup>4</sup> at 344 knots chamber velocity. This density has a bearing on the amount of aerodynamic moment available to cause oscillator vibration (reference Equation 8).

40. Figure 15 shows typical chamber velocity values at angles of attack for  $A_i/A_t = 5.5$  and  $\bar{A}_c/A_t = 9.5$  at an oscillator location of  $d = .280$  inches. At -6 degrees the chamber velocity started at 291 knots, at 2 degrees the minimum velocity was 282.4 knots and at 20 degrees the chamber velocity reached a maximum value of 302 knots.

From -6 to +2 degrees angle of attack the velocity relationship is not linear. The velocity is influenced primarily by the blockage in the tunnel due to the model position, sector arm, and to a lesser extent by a slight air flow inclination upstream at the supply end. These factors give a non-linear, higher velocity reading at negative and near zero angle of attack. As the model is rotated from +2 to positive angles of attack (up to +20°) the velocity is linear. A velocity value at -6° corresponds to a velocity value at +10° angle of attack. At 10° more of the sector arm is in the air flow causing increased blockage that gives a lower air speed. For summary figures like Figure 5 the values of chamber velocity were taken at near zero degrees angle of attack.

#### COMMENTS

41. One theory explaining the flutter mechanism that can be generated from the enclosed data will be called "region of energy gradient."

42. The basic premise for the flutter arming phenomenon is an aerodynamic lift working through a center of pressure relative to a pivot point and the relative magnitude of energy the air possesses. The nozzle establishes an energy region, i.e., region of changing velocity and pressure, that works on the oscillator through aerodynamic lift. The location of the energy region is influenced by the air forming a nozzle contour, aft of the nozzle, the presence and movement of the oscillator in the air flow, the magnitude of the air velocity at the inlet, and the magnitude of the back pressure.

43. If the oscillator is placed in a region of undisturbed constant flow the aerodynamic moment causing vibration is relatively low. This is characterized by the placement of the oscillator too far aft from the nozzle, out of the energy region. The energy gradient appears to move forward with increase in velocity allowing even less of the oscillator to be in the energy region.

44. Placing the leading edge of the oscillator close to the nozzle will place more of the oscillator in the region of energy gradient. A larger aerodynamic moment is witnessed and in turn an increasing frequency is established with an increase in velocity. Midway between the two extremes the frequency does not change with increased air velocity. The decrease in air density as velocity is increased will have a tempering effect tending toward a constant frequency response.

45. The FAM operation theory, "region of energy gradient", can best be described by an illustration. Figure 16 shows a qualitative diagram of the author's concept of this theory. Schlieren photography is planned in the near future to verify the flow concept. Note that the diagrams show the "energy region" with a stationary oscillator only. The flow pattern illustrated is typical for the various physically defined  $A_1/A_t$ ,  $\bar{A}_c/A_t$  ratios.

a. Figure 16a shows the relative location of the energy region and the oscillator location at or near the optimum location. When an inlet velocity ( $V_1$ ) is large enough to establish Mach ( $M$ ) = 1 at the throat,  $M > 1$  is established for a small distance downstream of the throat. Note that part of the air exiting from the nozzle forms a nozzle contour due to eddy flow and expansion conditions. The flow is then decelerated and a second shock wave or  $M = 1$  is established. The region bounded by the second shock wave to where the flow has reached steady state ( $V_1'$ ) is called the "energy gradient" region. For a greater inlet velocity ( $V_2$ ) the steady state region moves forward ( $V_2'$ ), accordingly the energy gradient region also moves forward, but since the oscillator is at or near the optimum location it remains within this region giving a constant frequency response.

b. Figure 16b shows the oscillator too far aft from the nozzle for effective use of the "energy region". As the "energy region" moves forward with increase of velocity the aerodynamic moment decreases until a non-vibrating condition exists.

c. Figure 16c has the oscillator too close to the nozzle exit. The second shock wave has been altered somewhat due to the presence of the oscillator. The "energy gradient" exists over a greater downstream distance allowing for a greater aerodynamic moment and increased frequency response. As the inlet velocity is increased the shape of the second shock wave becomes more concave and extends even further downstream. The aerodynamic moment increases to a value where the frequency response becomes very erratic.

46. The region of energy gradient for small inlet and chamber differences (4.53 and 5.2 respectively) appears to be quite short. Less of an allowable oscillator location deviation is permissible. At  $A_1/A_t = 5.6$  and  $A_c/A_t = 9.5$  the oscillator location is not as critical.

47. Another parameter that will influence the oscillator vibration is the throat area relative to the oscillator cross-section area. Unfortunately the data enclosed did not parametrically describe this variable. Although the throat area did vary somewhat from test to test no conclusions can be drawn.

#### CONCLUSIONS

48. The foregoing test results allow the following conclusions:

a. The frequency of vibration is the natural frequency of the oscillator-restoring member combination (no output load).

b. Rise time from 0 to the natural frequency for this model has an order of magnitude of .005 sec at threshold velocity.

c. There is an optimum oscillator location and nozzle configuration that gives constant frequency at all speeds above threshold, but below Mach 1 for free stream velocity and angles of

ttack. For this particular model the optimized conditions are shown in Figure 17.

d. It should be noted that for a constant frequency response the ratio of oscillator "d" downstream location to the oscillator thickness is 2.63. This ratio has been found to hold for other models.

e. Constant frequencies at all inlet air speeds below Mach 1 can be achieved even with air densities varying by 36% from that at threshold.

f. The rounded leading edge oscillator had a lower threshold velocity than the blunt.

g. The balanced half oscillator will function similar to the full oscillator but the starting velocity is higher.

h. There are specific lower limits for  $\bar{A}_c/A_t$  ratios for constant frequency oscillator response.

i. The method of setting the restoring spring moment equal to the aerodynamic moment to determine the minimum velocity for oscillator start-up is not accurate. It appears that an inlet velocity that establishes Mach 1 at the nozzle throat is the criterion for this configuration.

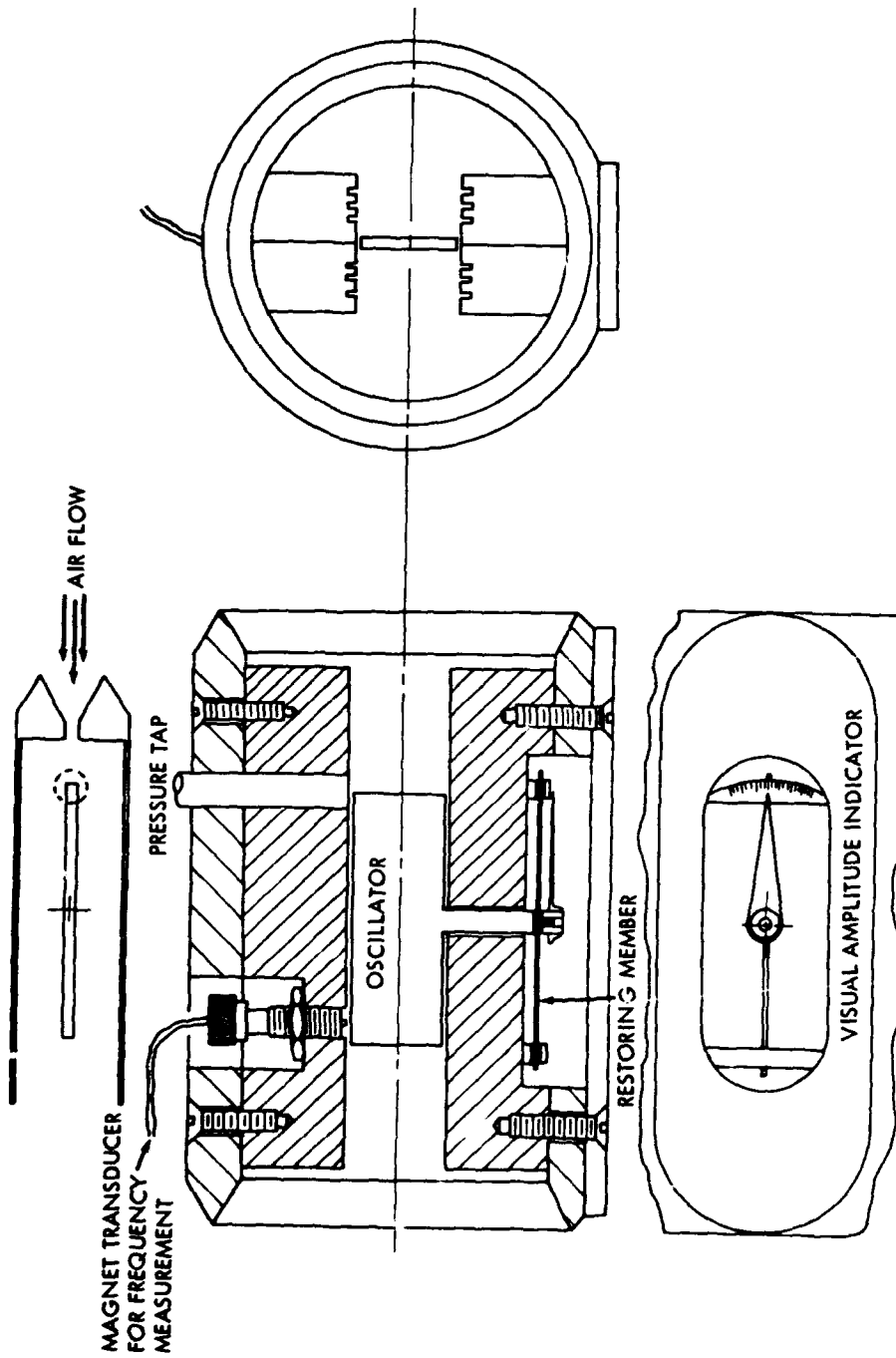


FIG.1 CONTROL VOLUME MODEL

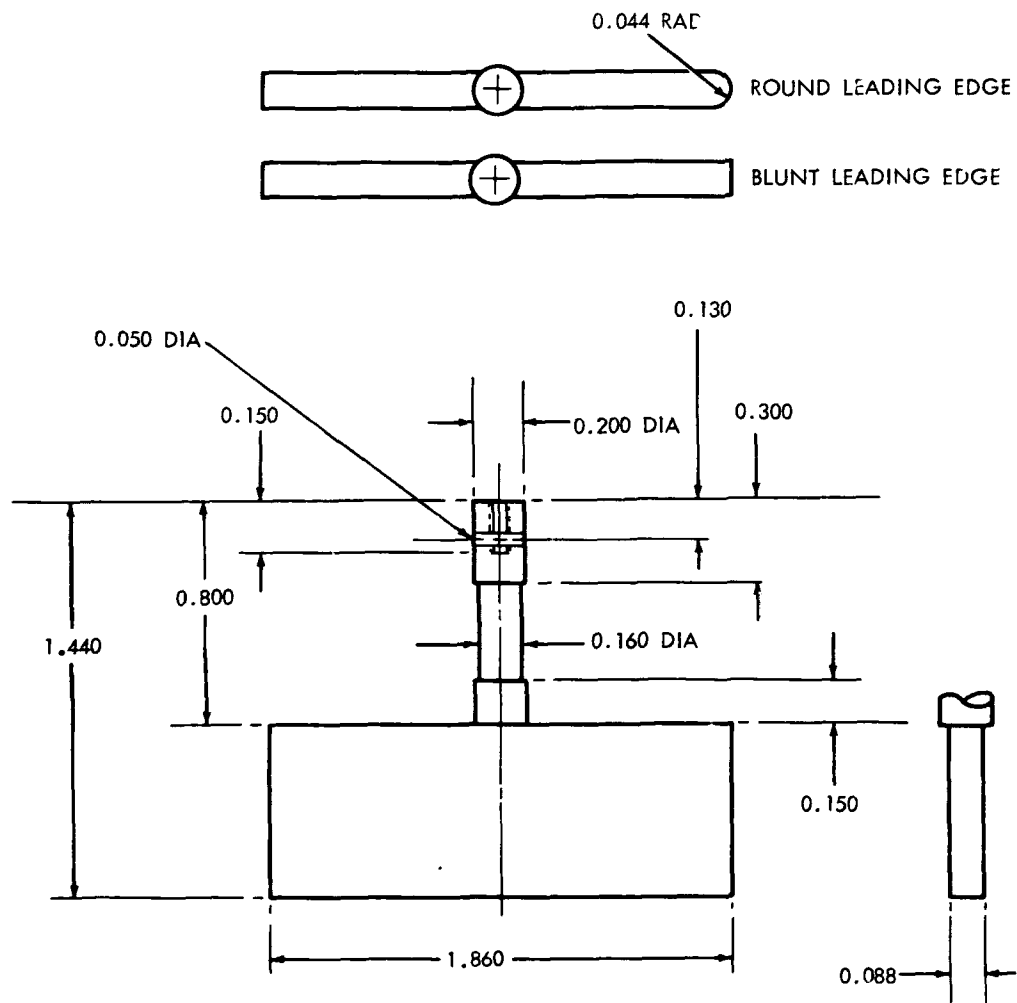


FIG. 2 OSCILLATOR CONFIGURATION

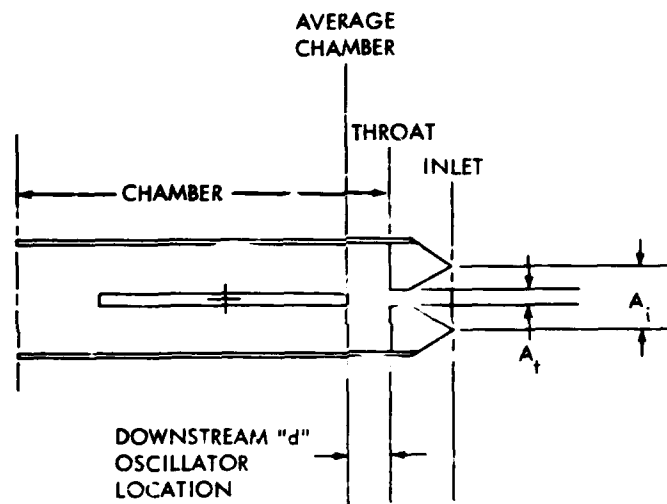


FIG. 3 SPACE LOCATIONS IN CONTROL VOLUME MODEL



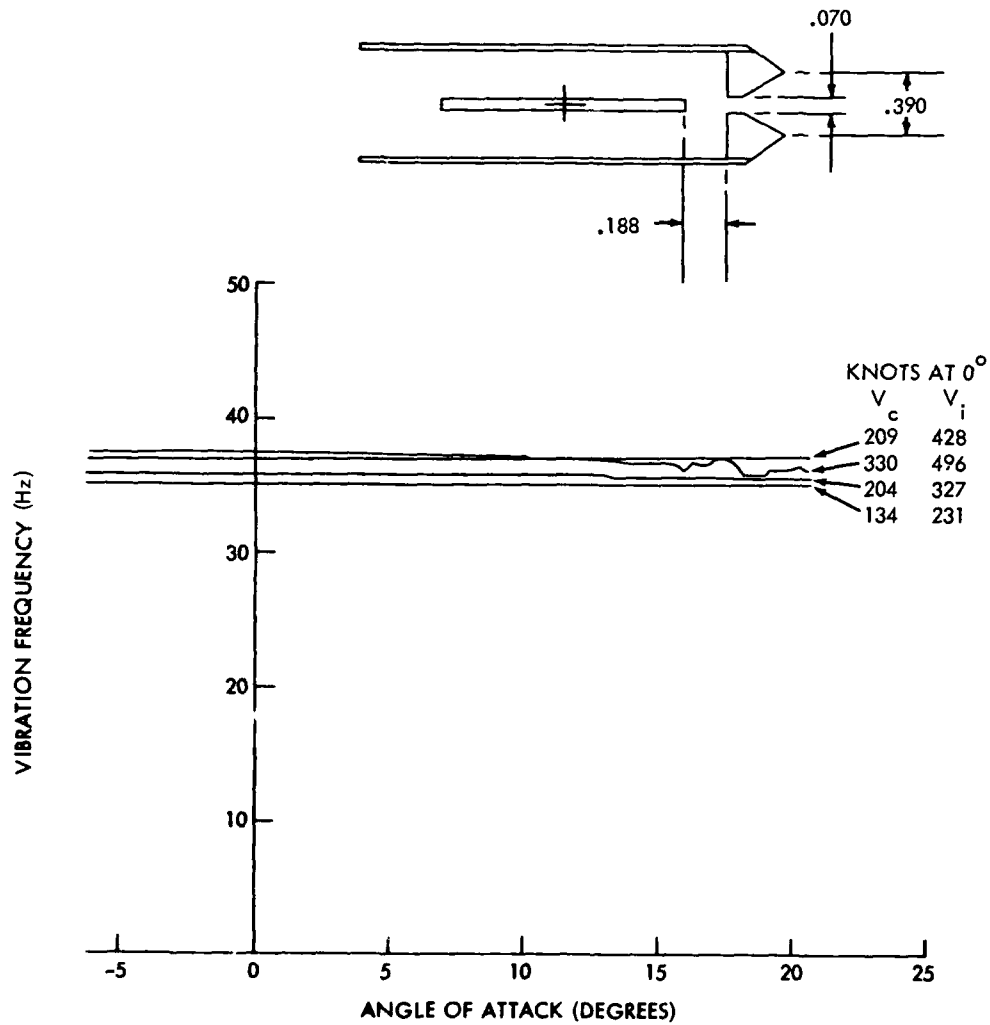


FIG.4 VIBRATION FREQUENCY VS ANGLE OF ATTACK FOR THE CONTROL VOLUME WITH 0.088 IN. BLUNT OSCILLATOR 0.188 IN. DOWNSTREAM OF CHAMBER THROAT ( $A_t$ ), FOR INLET RATIO,  $A_i/A_t = 5.57$  AND CHAMBER RATIO,  $A_c/A_t = 9.50$

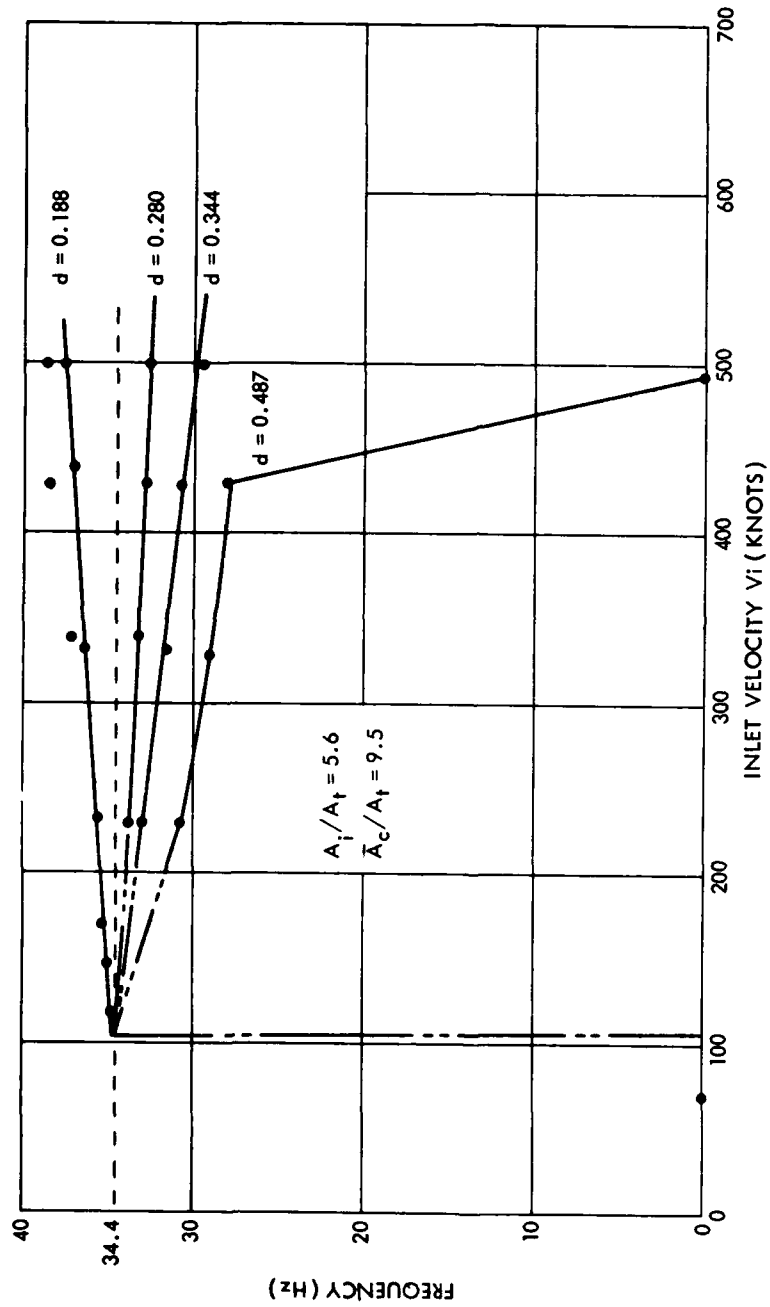


FIG. 5 FREQUENCY RESPONSE AS A FUNCTION OF OSCILLATOR LOCATION

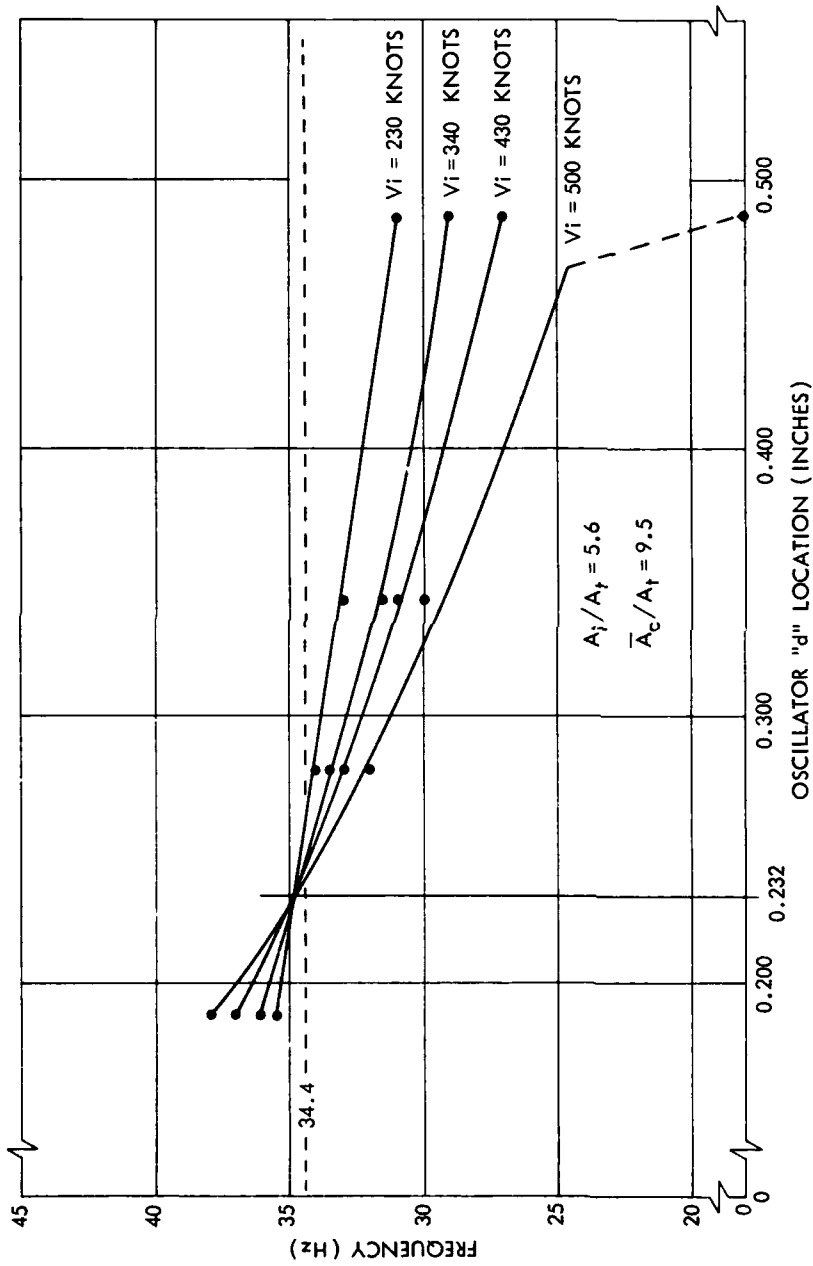


FIG. 6 OPTIMUM OSCILLATOR LOCATION FOR SPECIFIC  $A_i/A_t, A_c/A_t$  RATIOS

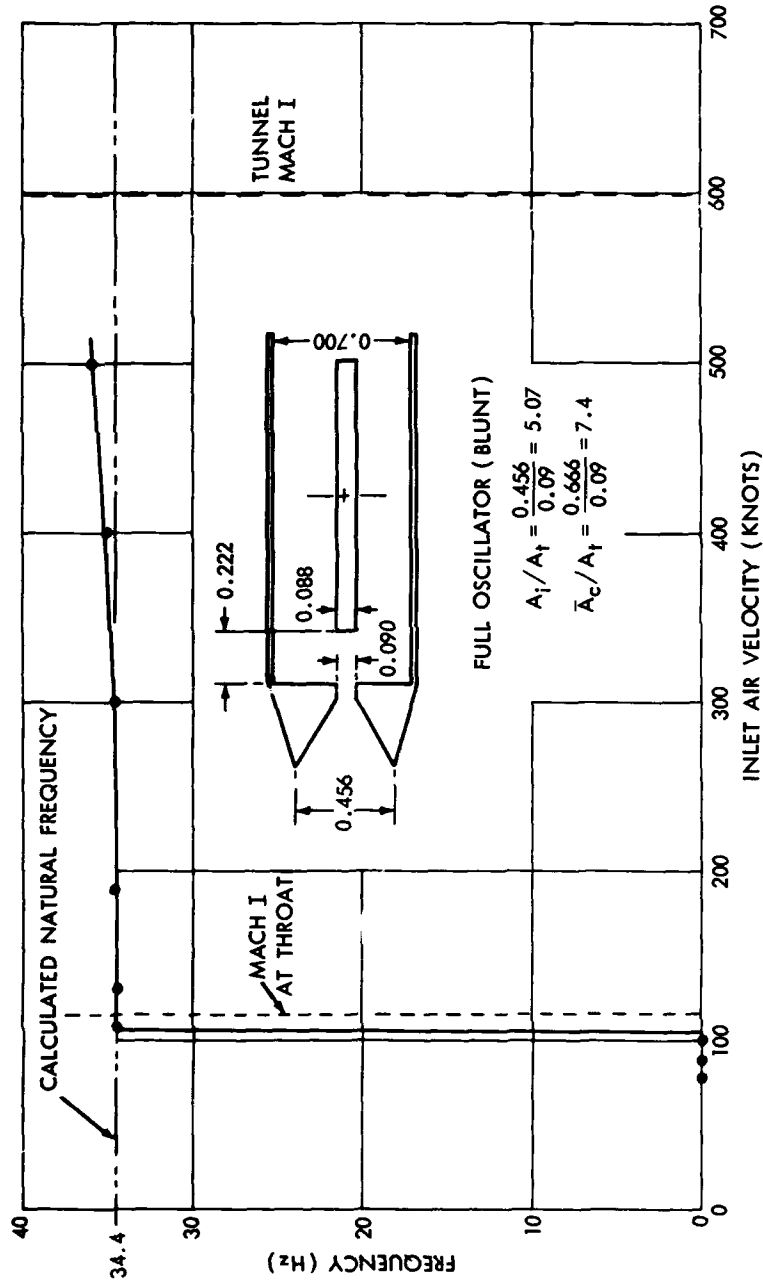


FIG. 7 FREQUENCY RESPONSE AT NEAR OPTIMUM LOCATION

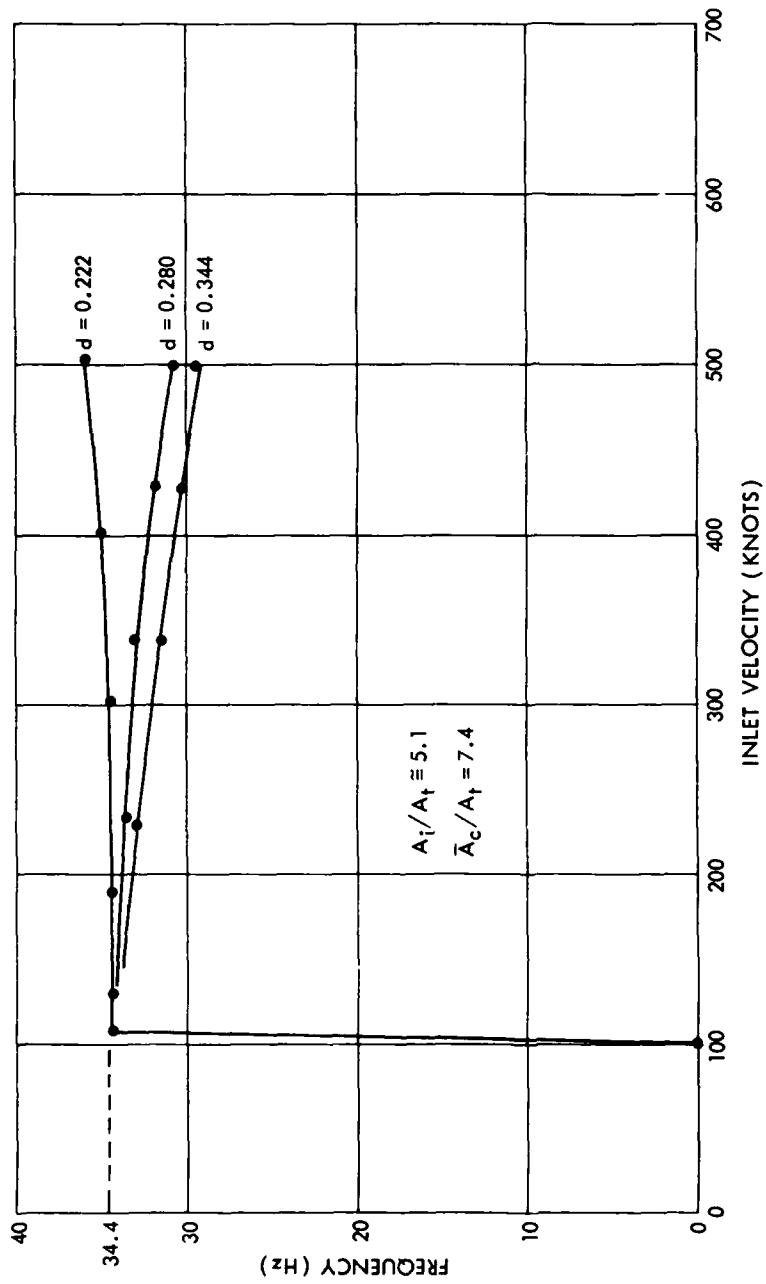


FIG. 8 FREQUENCY RESPONSE WITH OSCILLATOR DOWNSTREAM LOCATION  
AS PARAMETER FOR  $\bar{A}_c/A_t = 7.4$

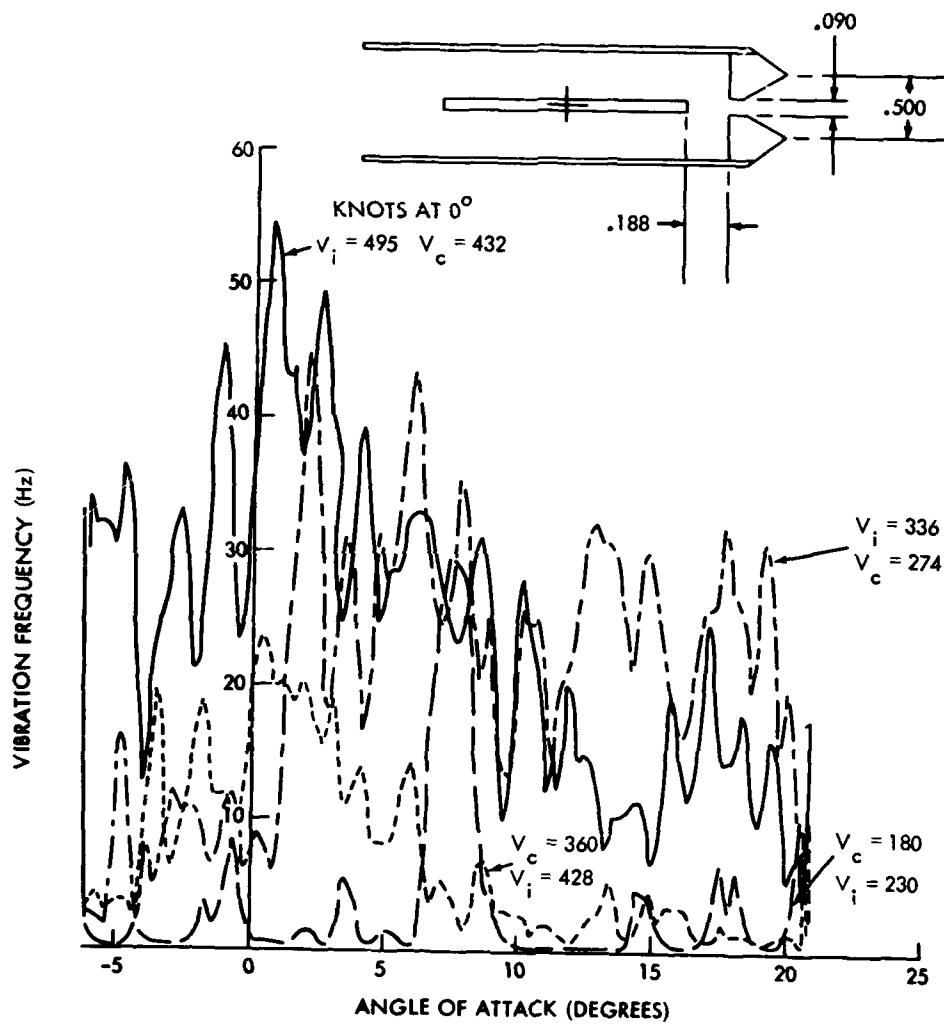


FIG. 9 VIBRATION FREQUENCY VS ANGLE OF ATTACK FOR THE CONTROL VOLUME WITH 0.088 IN. BLUNT OSCILLATOR 0.188 IN. DOWNSTREAM OF CHAMBER THROAT ( $A_t$ ), FOR INLET RATIO,  $A_i/A_t = 5.55$  AND CHAMBER RATIO,  $\bar{A}_c/A_t = 7.40$

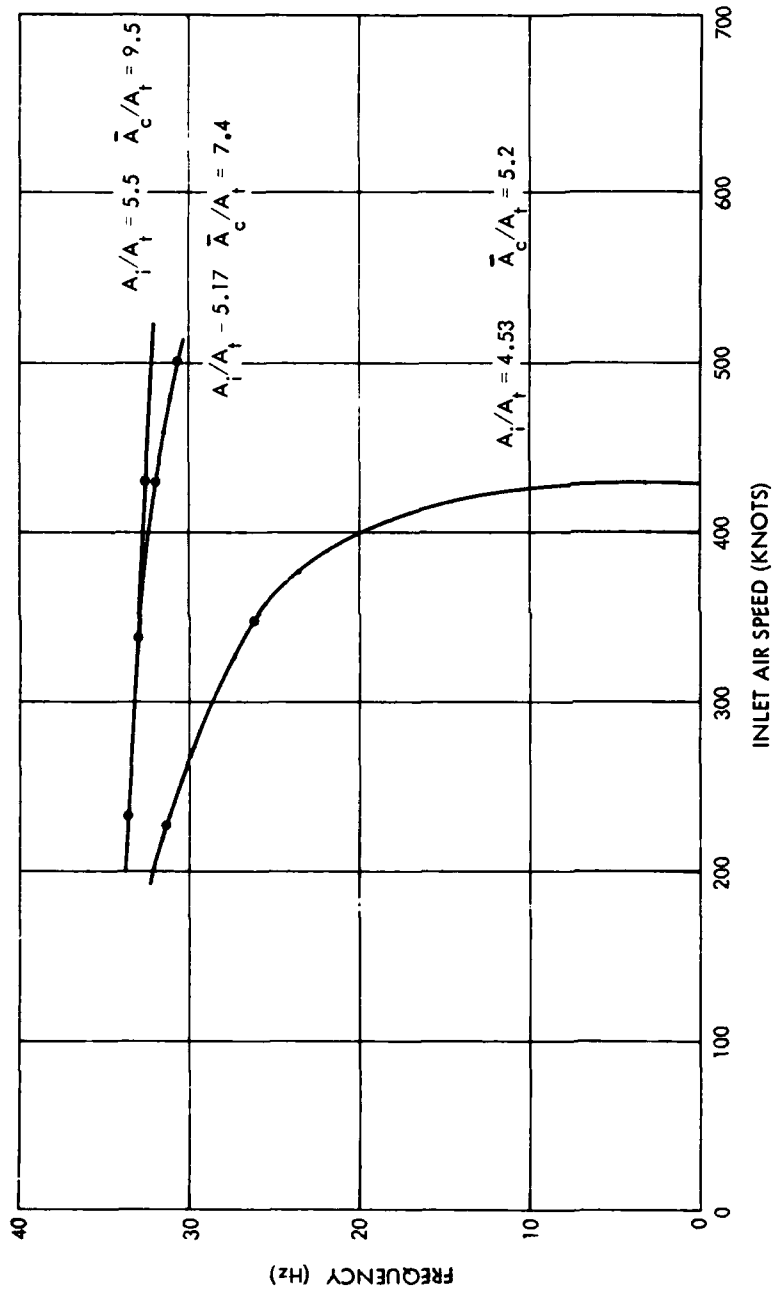


FIG. 10 FREQUENCY RESPONSE AT INLET AIR SPEEDS FOR RELATIVELY LITTLE CHANGE IN  $A_i/A_t$  RATIO BUT FOR LARGE DIFFERENCES IN  $\bar{A}_c/A_t$  RATIOS AT  $d=0.280$  IN.

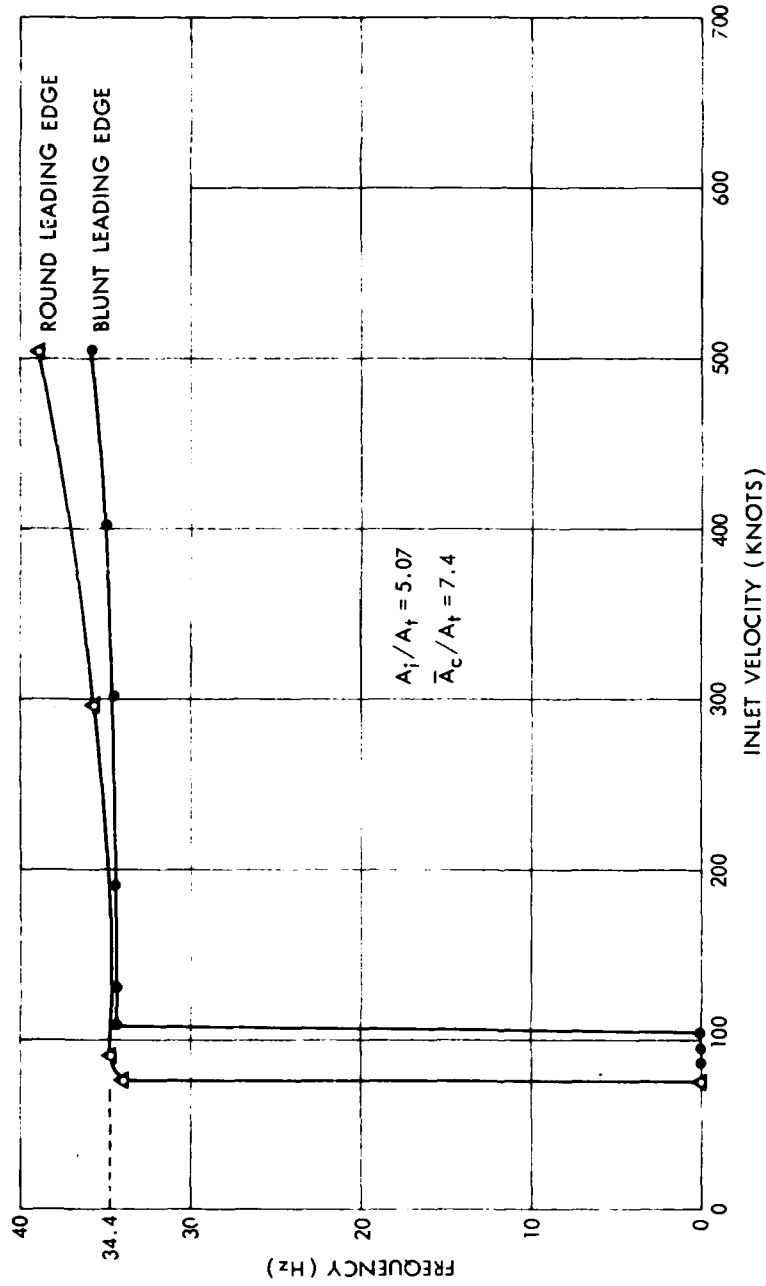


FIG. 11 FREQUENCY COMPARISON FOR BLUNT & ROUND LEADING EDGED OSCILLATOR



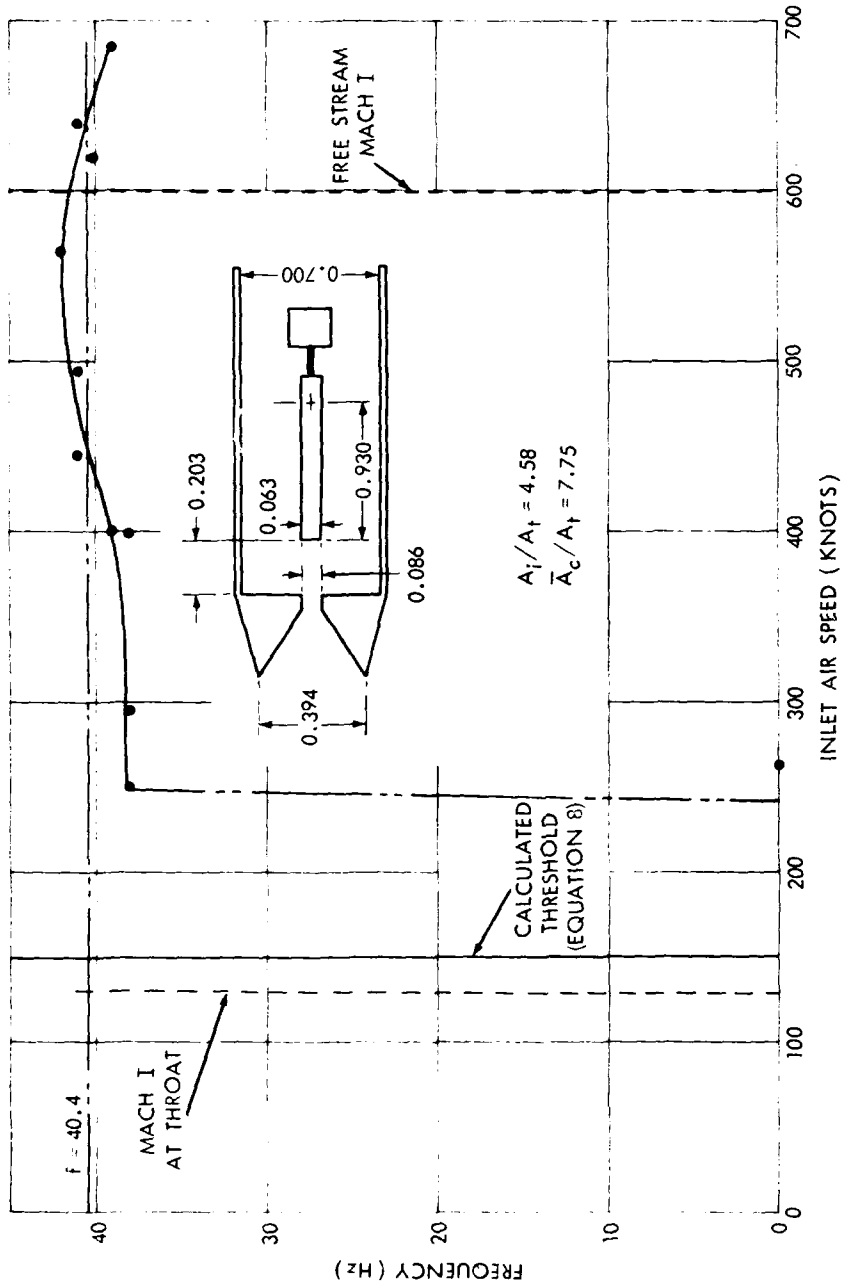


FIG. 12 FREQUENCY RESPONSE FOR ONE-HALF BALANCED OSCILLATOR

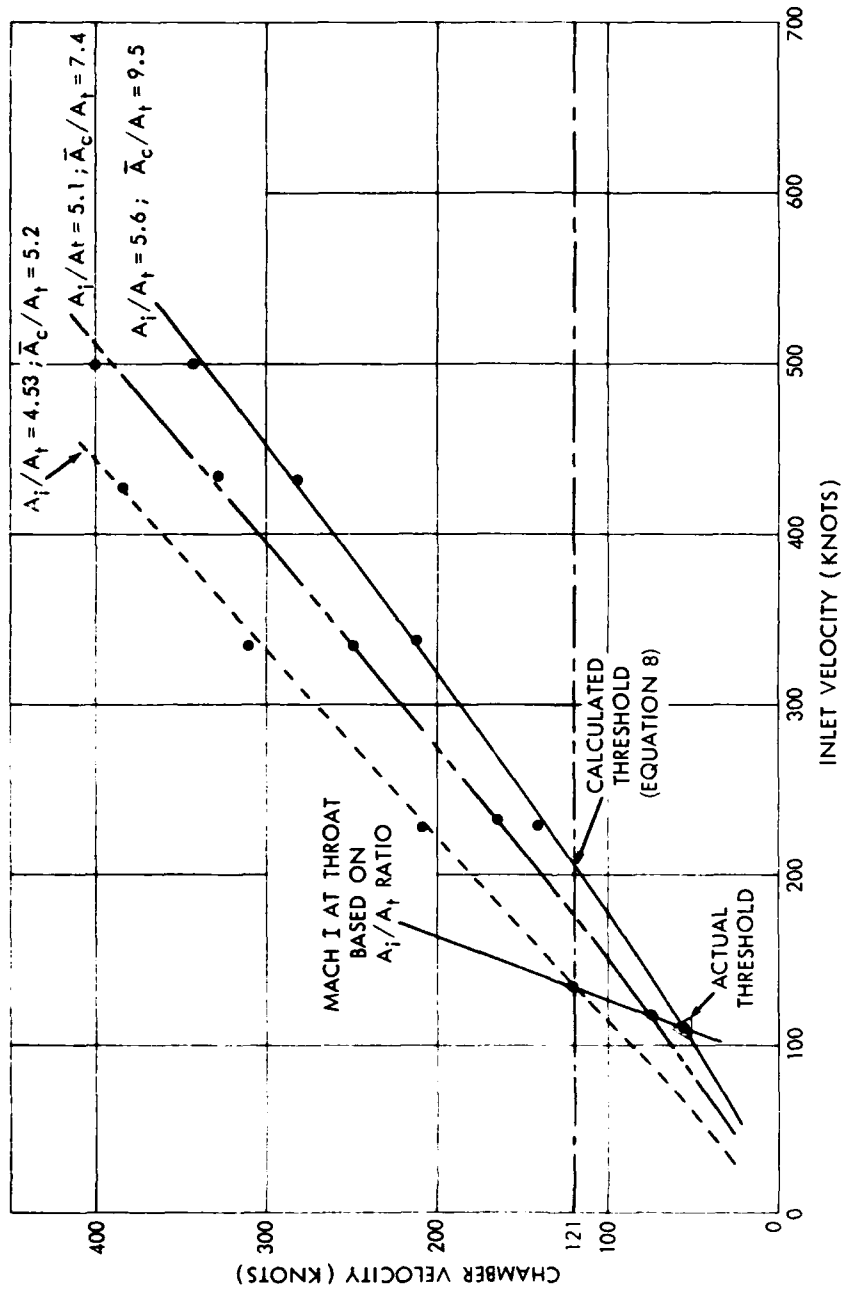


FIG. 13 CHAMBER VELOCITY VS INLET VELOCITY AS A FUNCTION OF  $A_1/A_t$  RATIOS

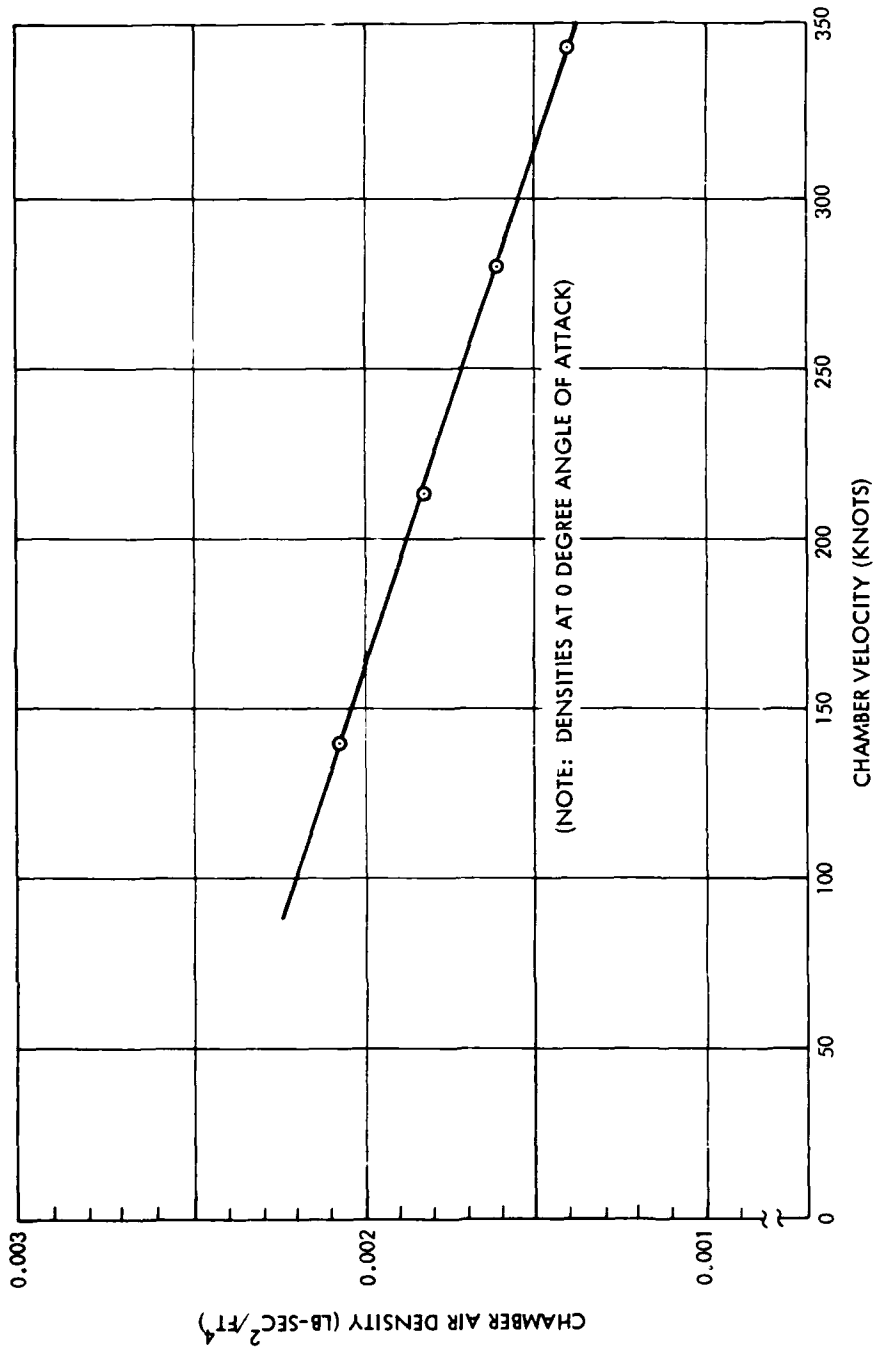


FIG. 14 CHAMBER AIR DENSITY VS CHAMBER AIR VELOCITY AT LEADING EDGE OF OSCILLATOR FOR  
 $A_1/A_2 = 5.60$  AND  $A_3/A_2 = 9.50$

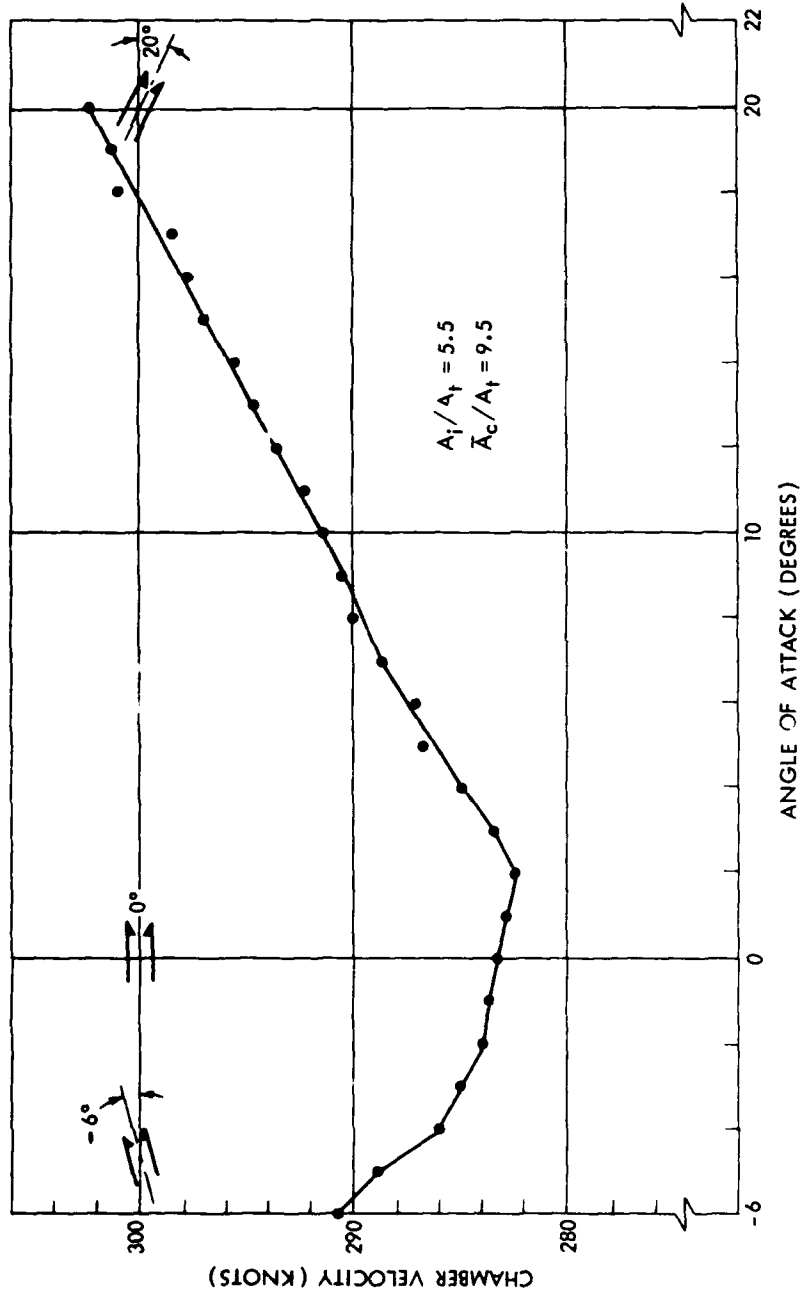


FIG. 15 TYPICAL CHAMBER VELOCITY RELATIONSHIP TO ANGLES OF ATTACK

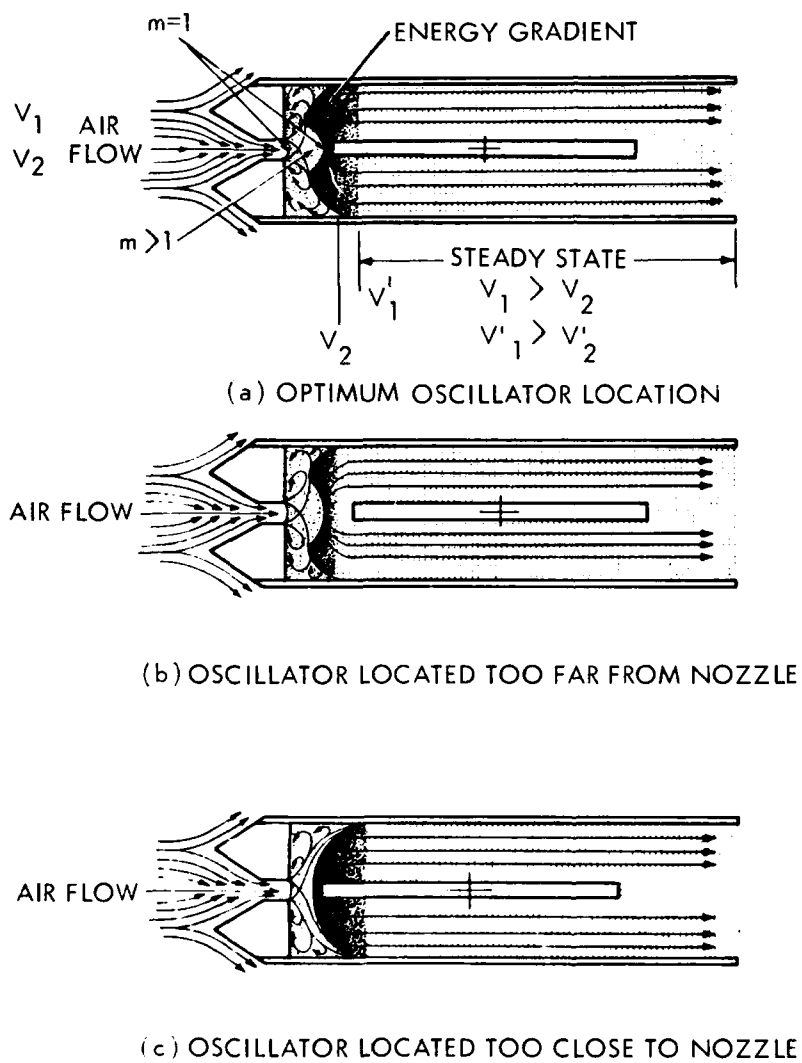
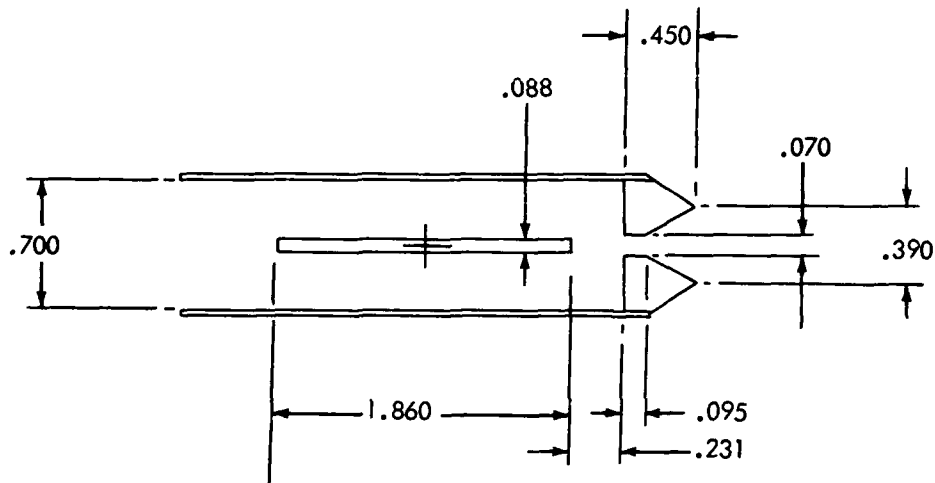


FIG. 16 ENERGY GRADIENT CONCEPT



CHAMBER HEIGHT = .725 IN

$$A_i/A_t = \frac{.390}{.070} = 5.6$$

$$\bar{A}_c/A_t = \frac{.700 - .034}{.070} = 9.5$$

$$A_c/A_t = \frac{.700}{.070} = 10.0$$

NOTE: .034 CORRECTION FOR STATIC PRESSURE PROBE

FIG. 17 OPTIMUM DIMENSIONS FOR CONTROL VOLUME MODEL  
FOR ONE PARTICULAR NOZZLE AND OSCILLATOR  
CONFIGURATION

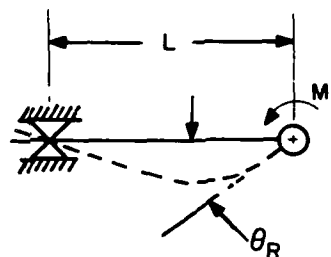
**BLANK PAGE**

APPENDIX A

Part 1.

From Reference (d);

$$\theta_R = \frac{M_1 L}{3 EI}$$



For the restoring member;

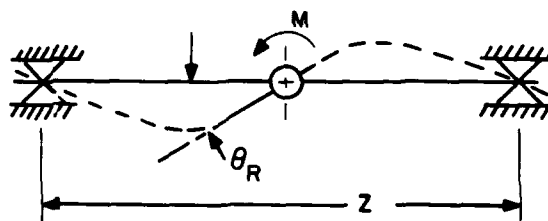
$$\theta_R = \frac{M_1 L}{3 EI}$$

$$\text{but } M_1 = M/2$$

$$L = Z/2$$

$$\therefore \theta_R = \frac{(M/2)(Z/2)}{3 EI}$$

$$\text{but } K = \frac{M}{\theta} = \frac{12 EI}{Z} \left( \frac{\text{lb-in}}{\text{Rad}} \right)$$





APPENDIX A

Part 2.

Threshold velocity for one-half, balanced, oscillator.

$$v_{cr}^2 = \frac{K}{\pi \rho_c \bar{S} \bar{a}} \quad \text{Equation (8)}$$

where  $S = .595 \text{ in}^2$  ( $\frac{1}{2}$  original oscillator area)

$$K = 102. \times 10^{-2} \text{ lb-in}$$

$$\bar{a} = .697 \text{ in } (3/4 \times .930)$$

$$\rho_c = 2.16 \times 10^{-3} \frac{\text{lb-sec}^2}{\text{ft}^4}$$

$$\therefore v_{cr} = \left[ \frac{1.02 (144)}{.595 \pi} \right]^{1/2} \sqrt{\frac{1}{\rho_c \bar{a}}}$$

$$= 8.85 \sqrt{\frac{1}{2.16 \times .697 \times 10^{-3}}}$$

$$= 228 \text{ ft/sec or 135 knots chamber}$$

APPENDIX B

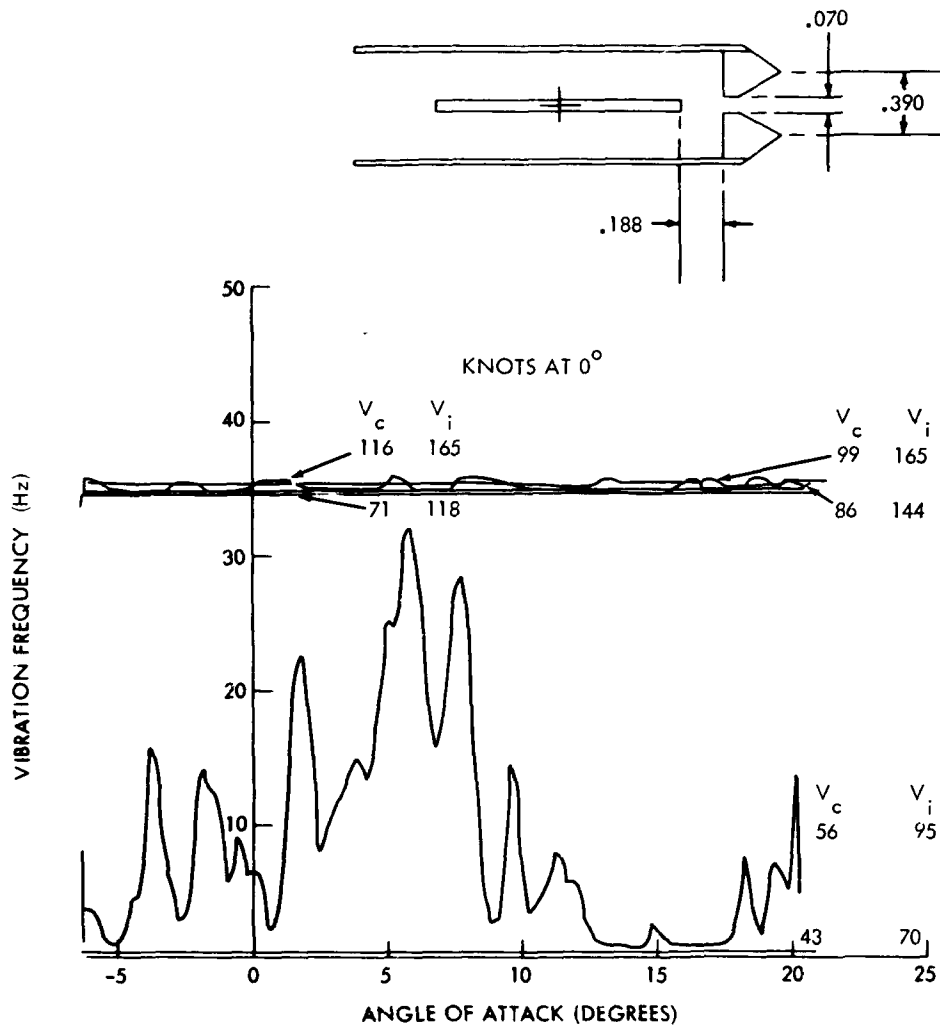


FIG. B-1 VIBRATION FREQUENCY VS ANGLE OF ATTACK FOR THE CONTROL VOLUME WITH 0.088 IN. BLUNT OSCILLATOR 0.188 IN. DOWNSTREAM OF CHAMBER THROAT ( $A_t$ ), FOR INLET RATIO,  $A_i/A_t = 5.57$  AND CHAMBER RATIO,  $\bar{A}_c/A_t = 9.50$

APPENDIX B

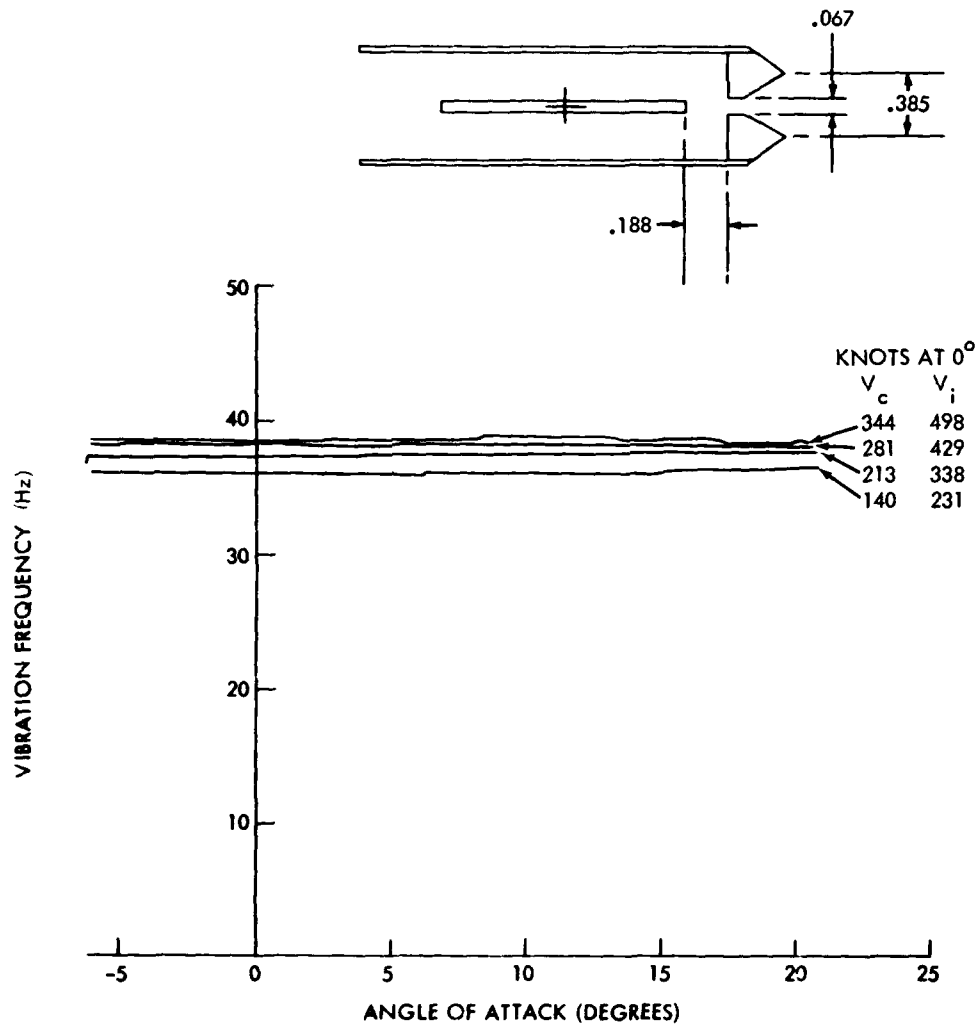


FIG. B-2 VIBRATION FREQUENCY VS ANGLE OF ATTACK FOR THE CONTROL VOLUME WITH 0.088 IN. BLUNT OSCILLATOR 0.188 IN. DOWNSTREAM OF CHAMBER THROAT ( $A_t$ ), FOR INLET RATIO,  $A_i/A_t = 5.79$  AND CHAMBER RATIO,  $\bar{A}_c/A_t = 9.94$

APPENDIX B

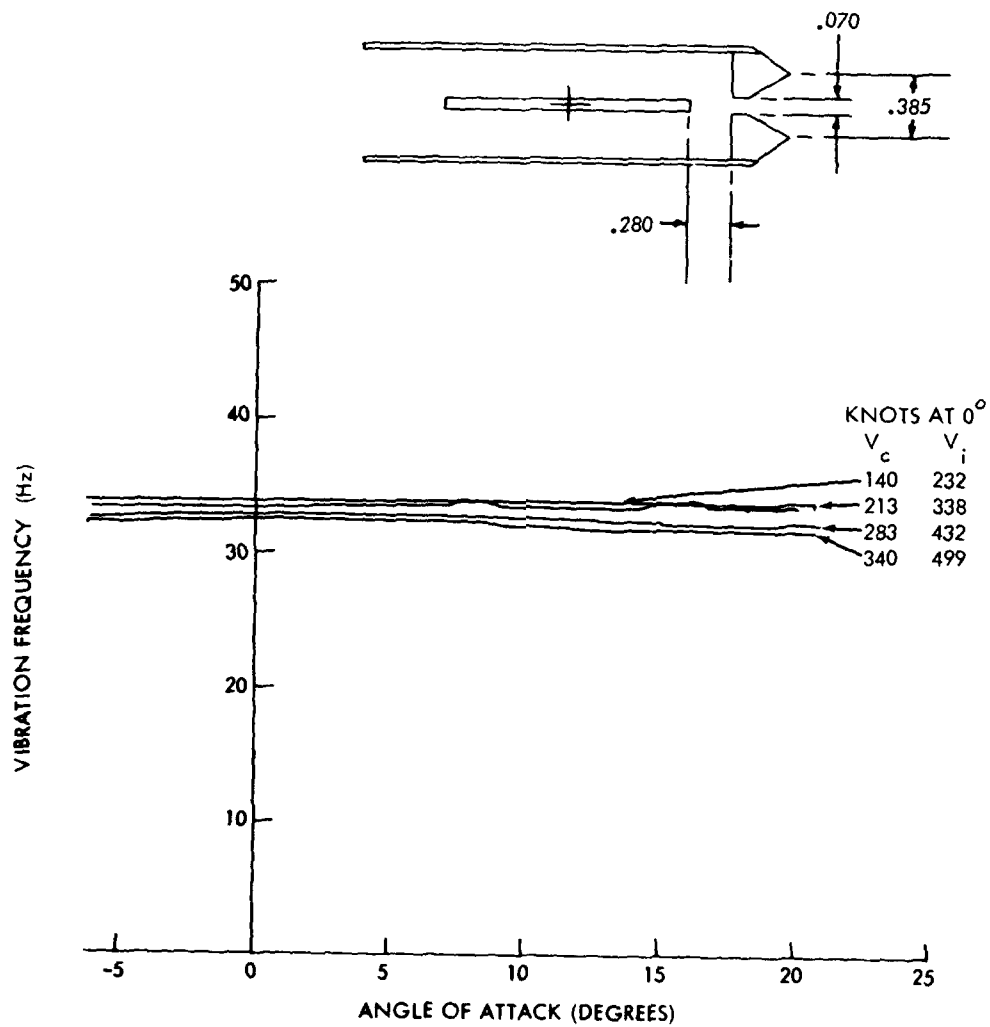


FIG. B-3 VIBRATION FREQUENCY VS ANGLE OF ATTACK FOR THE CONTROL VOLUME WITH 0.088 IN. BLUNT OSCILLATOR 0.280 IN. DOWNSTREAM OF CHAMBER THROAT ( $A_t$ ), FOR INLET RATIO,  $A_i/A_t = 5.50$  AND CHAMBER RATIO,  $\bar{A}_c/A_t = 9.50$

APPENDIX B

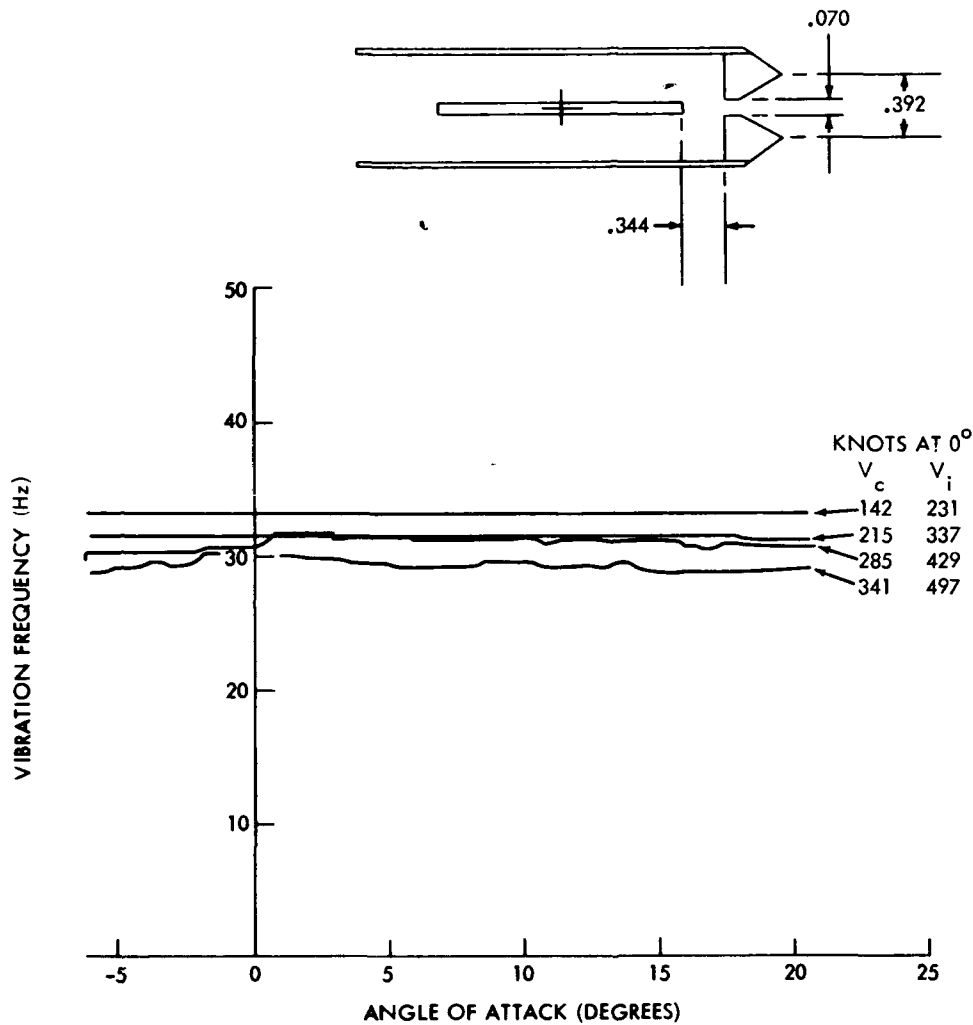


FIG. B-4 VIBRATION FREQUENCY VS ANGLE OF ATTACK FOR THE CONTROL VOLUME WITH 0.088 IN. BLUNT OSCILLATOR 0.344 IN. DOWNSTREAM OF CHAMBER THROAT ( $A_t$ ), FOR INLET RATIO,  $A_i/A_t = 5.60$  AND CHAMBER RATIO,  $\bar{A}_c/A_t = 9.50$

APPENDIX B

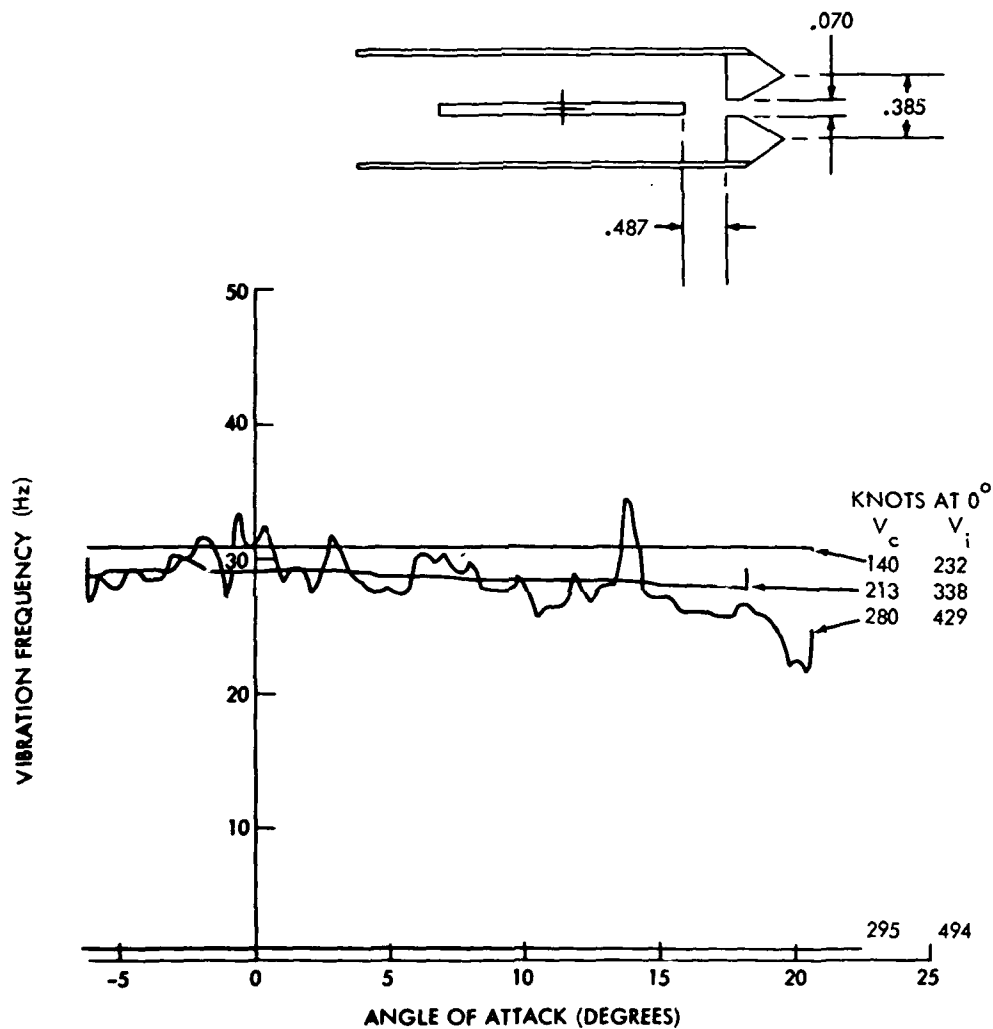


FIG. B-5 VIBRATION FREQUENCY VS ANGLE OF ATTACK FOR THE CONTROL VOLUME WITH 0.088 IN. BLUNT OSCILLATOR 0.487 IN. DOWNSTREAM OF CHAMBER THROAT ( $A_t$ ), FOR INLET RATIO,  $A_t/A_t = 5.50$  AND CHAMBER RATIO,  $\bar{A}_c/A_t = 9.50$

APPENDIX B

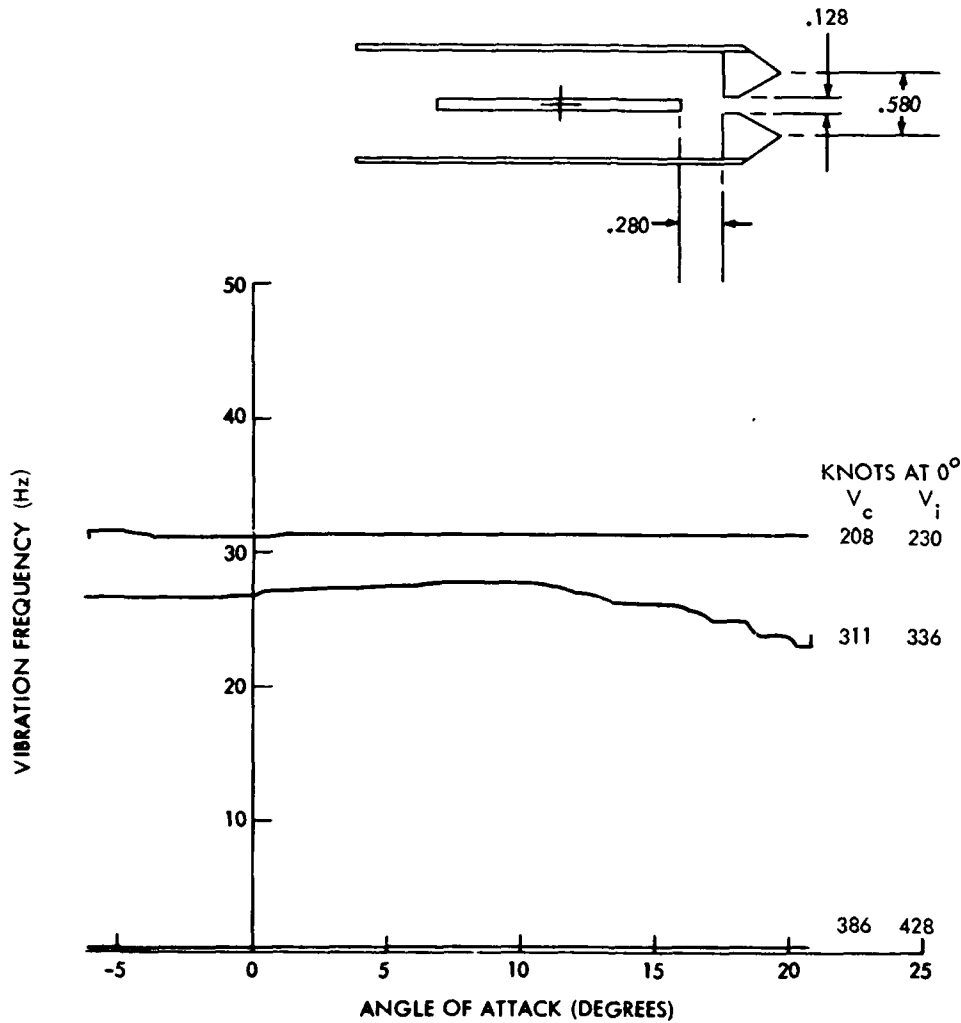


FIG. B-6 VIBRATION FREQUENCY VS ANGLE OF ATTACK FOR THE CONTROL VOLUME WITH 0.088 IN. BLUNT OSCILLATOR 0.280 IN. DOWNSTREAM OF CHAMBER THROAT ( $A_t$ ), FOR INLET RATIO,  $A_i/A_t = 4.53$  AND CHAMBER RATIO,  $A_c/A_t = 5.2$

APPENDIX B

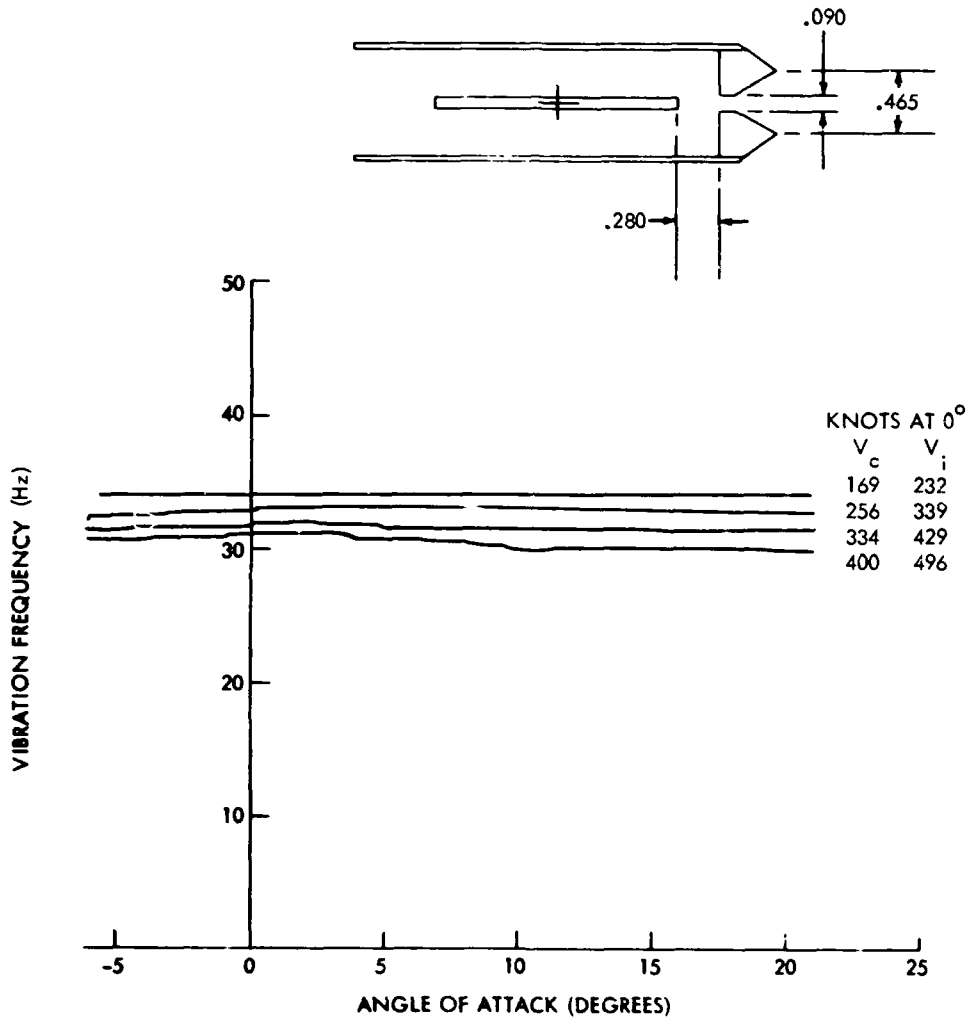


FIG. B-7 VIBRATION FREQUENCY VS ANGLE OF ATTACK FOR THE CONTROL VOLUME WITH 0.088 IN. BLUNT OSCILLATOR 0.280 IN. DOWNSTREAM OF CHAMBER THROAT ( $A_t$ ), FOR INLET RATIO,  $A_i/A_t = 5.17$  AND CHAMBER RATIO,  $\bar{A}_c/A_t = 7.40$



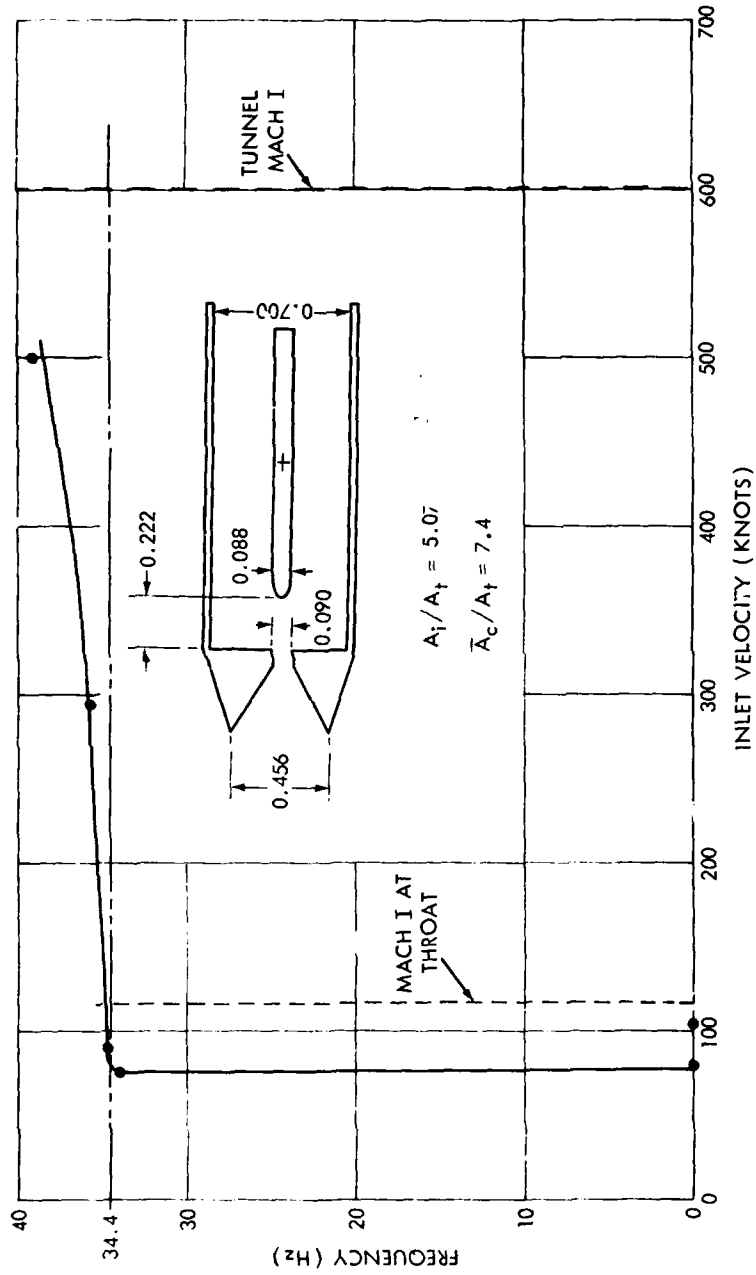


FIG. B-8 FREQUENCY RESPONSE FOR ROUND LEADING EDGE OSCILLATOR

UNCLASSIFIED

Security Classification

DOCUMENT CONTROL DATA - R & D		
Security Classification of title, body of abstract and indexing annotation must be entered when the overall report is classified		
1. ORIGINATING ACTIVITY (Corporate author)		2a. REPORT SECURITY CLASSIFICATION
U. S. Naval Ordnance Laboratory White Oak, Silver Spring, Maryland		UNCLASSIFIED
		2b. GROUP
3. REPORT TITLE		
Preliminary Parametric Study of the Flutter Arming Principle for Fuzes		
4. DESCRIPTIVE NOTES (Type of report and inclusive dates)		
R&D through 8 Sep 1967		
5. AUTHOR(S) (First name, middle initial, last name)		
Peter D. Gratton		
6. REPORT DATE	7a. TOTAL NO. OF PAGES	7b. NO. OF REFS
11 September 1967	44	5
8. CONTRACT OR GRANT NO.		9a. ORIGINAL REPORT NUMBER(S)
AIRTASK A35-532-006/292-1/F008-08-07		NOLTR 67-144
b. PROJECT NO.		9b. OTHER REPORT NO(S) (Any other numbers that may be assigned this report)
c.		
d.		
10. DISTRIBUTION STATEMENT		
This document is subject to special export controls and each transmittal to foreign governments may be made only with prior approval of NOL.		
11. SUPPLEMENTARY NOTES		12. SPONSORING MILITARY ACTIVITY
		Naval Air Systems Command
13. ABSTRACT		
<p>The Flutter Arming Mechanism (FAM) principle is a controlled flutter phenomenon. A rectangular flat plate oscillating member is pivoted about its midchord on a member providing a flexural restoring moment. Placed edgewise in an air stream, the system is in unstable-stable equilibrium; at a predetermined air speed or above, aerodynamic lift on the front portion of the flat plate overcomes the flexural resisting moment and the oscillator vibrates. The vibrations occur at the natural frequency of the oscillator-torsion member combination. Wind tunnel data are presented which indicate the FAM principle has the necessary criterion of a time base, velocity discriminating mechanism required for bomb and bomblet fuze application.</p>		

DD FORM 1473

1 NOV 65

(PAGE 1)

UNCLASSIFIED

Security Classification

S/N 0101-807-6801

UNCLASSIFIED

Security Classification

KEY WORDS	LINK A		LINK B		LINK C	
	ROLE	WT	ROLE	WT	ROLE	WT
Flutter Arming Mechanism						
Controlled Flutter						
Oscillating Flat Plate Between Parallel Walls						
Oscillating Vane Between Parallel Walls						
Vibrating Flat Plate Between Parallel Walls						
Bomb Fuze						
Bomblet Fuze						
Velocity Discrimination						
Time Base Mechanism						

D FORM 1473 (BACK)  
NOV 68  
(GE 2)

UNCLASSIFIED

Security Classification